

## **Virtual and Physical Prototyping**



ISSN: 1745-2759 (Print) 1745-2767 (Online) Journal homepage: www.tandfonline.com/journals/nvpp20

# Bio-derived PA11/bamboo charcoal/glass fibre composites for fused filament fabrication, warpage control, strength and flame retardancy

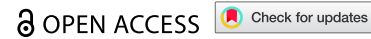
Kaveh Rahmani, Callum Branfoot & Mahdi Bodaghi

**To cite this article:** Kaveh Rahmani, Callum Branfoot & Mahdi Bodaghi (2025) Bio-derived PA11/bamboo charcoal/glass fibre composites for fused filament fabrication, warpage control, strength and flame retardancy, Virtual and Physical Prototyping, 20:1, e2589848, DOI: 10.1080/17452759.2025.2589848

To link to this article: <a href="https://doi.org/10.1080/17452759.2025.2589848">https://doi.org/10.1080/17452759.2025.2589848</a>

9	© 2025 The Author(s). Published by Informa UK Limited, trading as Taylor & Francis Group
	Published online: 24 Nov 2025.
	Submit your article to this journal 🗗
a <sup>r</sup>	View related articles 🗗
CrossMark	View Crossmark data ☑ ੈ







### Bio-derived PA11/bamboo charcoal/glass fibre composites for fused filament fabrication, warpage control, strength and flame retardancy

Kaveh Rahmani<sup>a</sup>, Callum Branfoot<sup>b</sup> and Mahdi Bodaghi <sup>©</sup>

<sup>a</sup>Department of Engineering, Nottingham Trent University, Nottingham, UK; <sup>b</sup>Engineering Operations, NCC, Bristol, UK

#### **ABSTRACT**

Adoption of polyamide-11 (PA11) in fused-filament fabrication (FFF) has been limited by warpage, trade-offs between stiffness/strength and toughness at service temperatures, and reliance on nonsustainable flame-retardant packages. To address these challenges, a bio-derived library of PA11 composites was formulated and FFF-printed by compounding bamboo charcoal (BC, 0-5 wt.%) with or without glass fibre (GF, 30 wt.%). Filaments were extruded and specimens were characterised for warpage, wettability, thermo-mechanical response, flammability, mechanical performance (tensile/flexural/impact/hardness) from 23-90°C. Warpage suppressed from 3.81 mm in PA11 to  $\sim$ 0.1 mm with 3 wt.% BC + 30 wt.% GF ( $\sim$ 97% reduction), indicating effective shrinkage control during printing. Mechanical performance was elevated: ultimate tensile strength reached 76.5 MPa in the hybrid, with increased hydrophobicity and improved high-temperature stiffness retention. Horizontal burning rate was lowered by up to 61.9% versus PA11, evidencing char-forming and barrier effects of BC with GF. Architected honeycomb meta-bio-composites were also printed, exhibiting quasi-zero-stiffness force regulation and high specific energy absorption (655 J/kg at 50% compression), highlighting utility for energy dissipators and overload protection. Sustainable, FFF-printable PA11/BC/GF formulations are therefore evidenced to deliver lightweight, durable candidates for automotive, robotic, and protective-sport applications while clarifying processing - structure - property relationships for functional PA11.

#### **ARTICLE HISTORY**

Received 1 October 2025 Accepted 11 November 2025

#### **KEYWORDS**

Bio-based polyamide 11; glass fibre; 3D printing; flammability; meta-biocomposite

#### 1. Introduction

Growing environmental concerns are shifting research and industry toward recyclable, renewable-source materials. In line with this trend, the use of sustainable thermoplastics and natural reinforcements is rapidly gaining importance, especially in industrial sectors where traditional carbon- and glass-fibre-reinforced thermosets have long been dominant (e.g. aerospace, marine, and construction) [1]. However, natural reinforcements and low-impact plastics often suffer from inferior performance, and their combination typically results in 'green composites' that may fail to meet the necessary requirements for many high-tech applications [2]. The key challenge lies in identifying new material combinations to produce high-performance green composites that can viably replace conventional options in suitable applications. Among the various thermoplastics explored for sustainable composites polyamides (nylons) are particularly attractive due to their strength, stiffness, and heat resistance across automotive, sport, robotic, and engineering applications [3,4].

This study focuses on Polyamide-11 (PA11), a semi-crystalline nylon made from castor-oil-based 11-aminoundecanoic acid. Because it comes from plant oil rather than petroleum, it helps cut fossil use and tends to lower the carbon footprint. Figure 1 groups common polymers by source and biodegradability. PA11 falls in the 'bio-based, non-biodegradable' group, together with other biobased polyamides and materials like PE, PET, and PTT. PA11 does not biodegrade in normal conditions while its renewable origin reduces overall environmental impact and provides a 100% bio-based option with high-performance engineering properties [5]. Moreover, compared with Nylon 6 and Nylon 6,6, PA11 absorbs less moisture, has higher impact resistance, and shows good chemical resistance to fuels, greases, and salts. While it usually costs more, this balance of mechanical strength and chemical durability has driven growing industrial use in the last decade [4,6]. PA11 is also stiffer than many other bio-based thermoplastics, such as PLA [7].

PA11 is reinforced with various fibres in different ways, including glass and carbon, for high strength

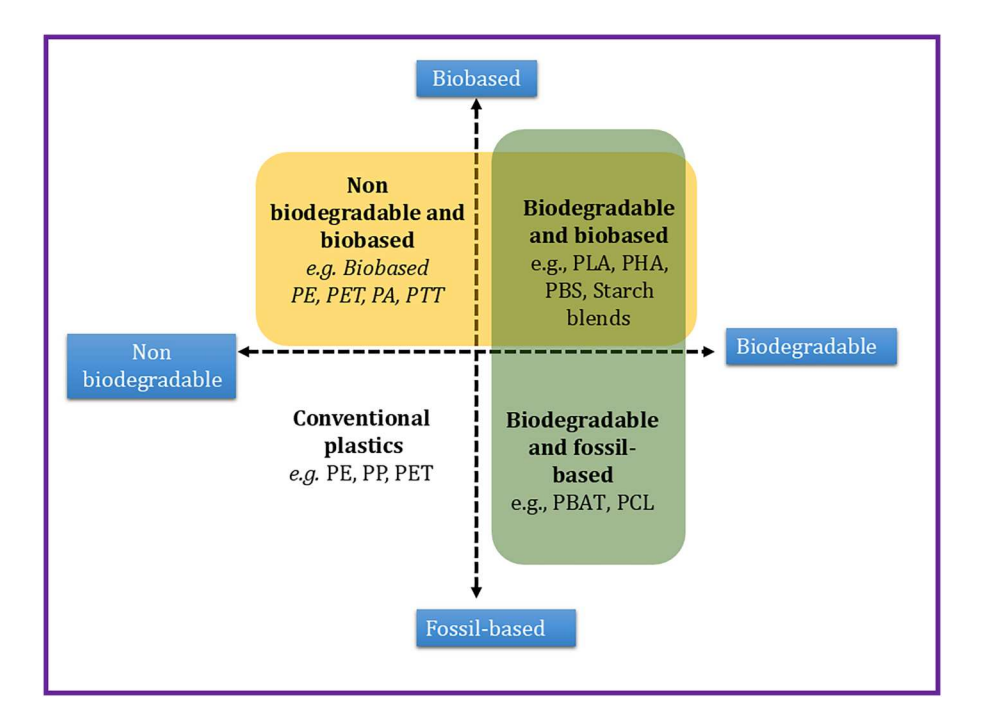


Figure 1. Classification of polymers by origin and biodegradability.

and excellent performance. Autay et al. [8] demonstrated that adding short glass fibres (GF) to polyamides produced by injection moulding raises both tensile and flexural strengths through improved load transfer and stiffness imparted by the fibres. Dechet et al. [9] showed that, in PA11/GF composites fabricated by selective laser sintering, increasing glass-fibre content leads to higher tensile strength, evidencing a positive, composition-dependent reinforcement effect. Bagrov et al. [10] showed that electrospun Nylon-11 mats achieve water contact angles up to  $126 \pm 2^{\circ}$  at 20% fibre coverage, indicating strong surface hydrophobicity. Mattos et al. [11] reported that the mechanical strength of polyamides fabricated by injection moulding decreases as temperature increases, reflecting the thermal softening and enhanced viscoelastic relaxation of the matrix. Demand for flame-retardant materials is rising across automotive, aerospace, transport, and construction, but many conventional additives (halogenated, phosphorus-based) have been banned in the EU since 2021 due to environmental and health risks, and can also weaken mechanical properties, prompting a search for sustainable alternatives [12,13]. Bamboo charcoal (BC) is attractive for safe and sustainable composites due to its abundance, rapid growth, mechanical strength, and compatibility [6,14]. Notably, BC can enhance flame resistance in thermoplastics. For example, Wu et al. [15] used powdered bamboo fibres as a charring agent in thermoplastic polyurethane (TPU) to achieve an 86% reduction in peak heat release rate versus pure TPU, supporting its use in fire-safe consumer and industrial products. Also, BC can enhance water resistance in thermoplastics. Chen et al. [16] added up to 12 wt.% BC to low-density polyethylene (LDPE), improving water resistance and contact angle. Sergi et al. [17] developed low-molecular-weight bio-PA11 composites reinforced with flax and intraply flax/basalt hybrid fabrics for eco-friendlier transportation components, reporting improved tensile strength, stiffness, and processability while maintaining a sustainable material profile. In a related study, Oliver-Ortega et al. [18] evaluated the thermal and thermomechanical behaviour of bio-based PA11 composites reinforced with lignocellulosic fibres. They reported enhanced stiffness and dimensional stability at elevated temperatures, confirming the potential of natural fibre reinforcement to improve heat resistance in sustainable polyamides. In this study, GF was intentionally used as a mechanical benchmark rather than a green reinforcement, to provide a reliable reference for assessing the contribution of the BC additive [19,20]. Comparing the bio-derived BC system with the established PA11/GF composite allows the hybrid formulation (PA11/3 wt.% BC/30 wt.% GF) to facilitate a straightforward and fair comparison between bio-based and conventional reinforcement options. This highlights BC potential to supplement or partly replace non-renewable fibres while still offering competitive mechanical and thermal performance. Moreover, PA11 products in the industry are primarily mass-produced through injection moulding. These routes excel at scale but require hard

tooling and long lead times, making rapid repeat and on-site spares impractical [8,11,21]. In contrast, composite additive manufacturing (AM), notably fused filament fabrication (FFF) is tool-free and CAD-driven, enabling fast, low-cost builds and quick design changes. Also, it is increasingly used for creating sustainable, high-performance functional parts and prototypes across many sectors such as automotive, construction, and sports [6,22,23].

Additive manufacturing of PA11 for functional parts faces concurrent requirements for high strength and stiffness, effective energy dissipation, and flame retardancy, alongside FFF-specific issues such as interlayer anisotropy and warpage. Existing studies on PA11 and related polyamides frequently optimise a single attribute (mechanical performance or flammability) and may rely on additives that compromise sustainability or printability [24,25]. In this context, bamboo charcoal merits attention as a bio-derived, char-forming particulate capable of acting as a heat sink, barrier former, and surface-energy modifier, while glass fibre is recognised for enhancing stiffness, strength, and dimensional stability. What remains insufficiently resolved for FFFprinted PA11 is how these reinforcements, individually and in concert, may influence processing-structureproperty relationships, hydrophobicity, and thermomechanical behaviour across service temperatures, and whether their use can mitigate warpage without sacrificing performance. These challenges motivate a systematic, application-oriented mapping of compositions and architectures for FFF, together with a fair comparison against conventional fabrication routes.

To address these needs, a bio-derived materials library of FFF-printable PA11 composites reinforced with BC, GF, and hybrid BC/GF formulations is established, spanning filament preparation, printing, and characterisation. Warpage, microstructure, wettability (water contact angle), thermo-mechanical behaviour, flammability, and principal mechanical properties (tensile, flexural, impact, and hardness) are quantified at ambient and elevated temperatures. The results show that BC and GF act synergistically to reduce deformation during printing, enhance hydrophobicity and flame resistance, and raise stiffness/ strength and energy dissipation. Moreover, an architected meta-bio-composite is realised that exhibits constant-force regulation and quasi-zero stiffness for efficient energy dissipation. Figure 2 summarises the development workflow from materials preparation to exemplar application

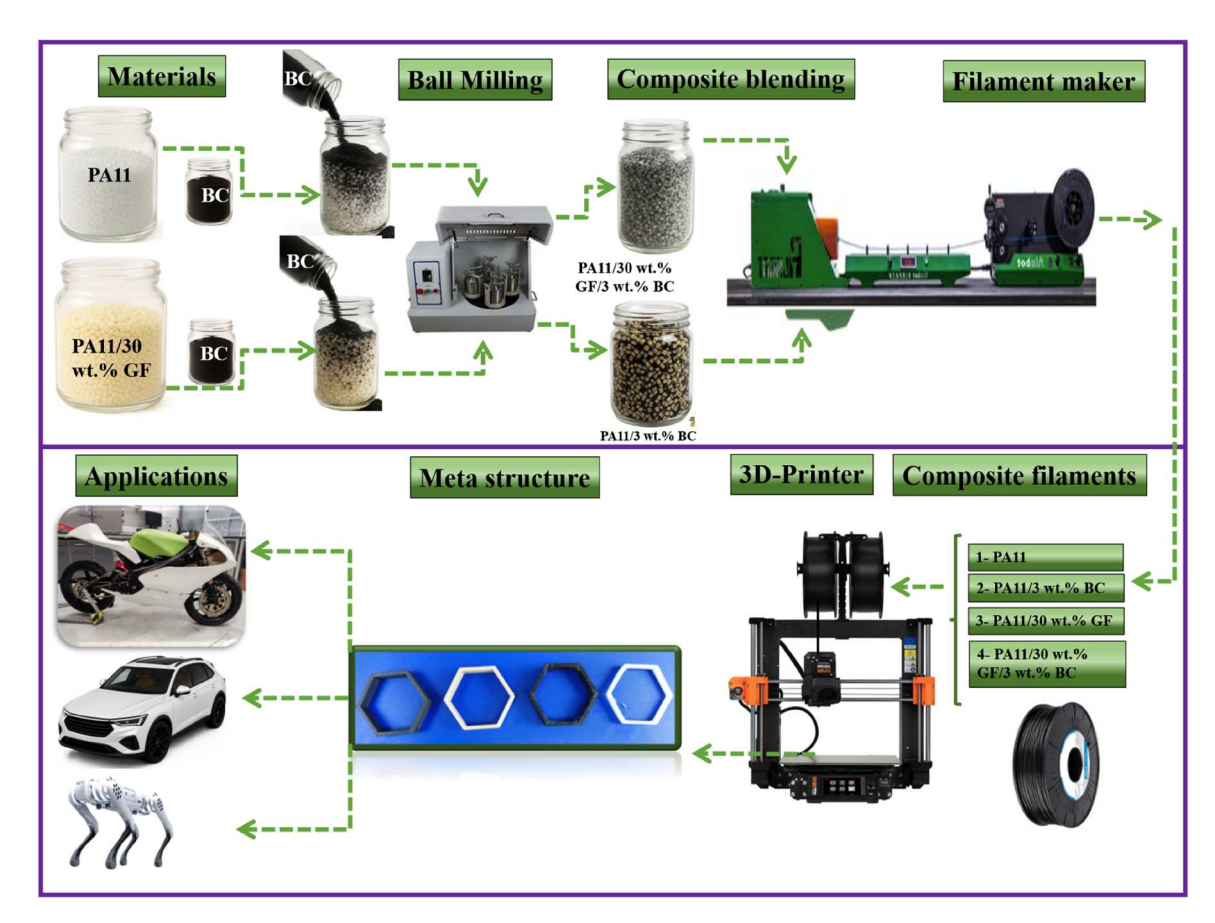


Figure 2. PA11 bio-composite production, from material preparation and extrusion to FFF 3D printing of meta-structures. Potential applications include components of robots, motorcycles, and automobiles.

domains, providing actionable guidance on formulations and scenarios in which FFF offers advantages for PA11 components.

#### 2. Bio-composite materials, manufacturing and testing

#### 2.1. Bio-compounds and composite constituents

In this research, bio-based PA11 and PA11/30 wt.% GF pellets were used as the matrix material (Figures 3(a and b)). PA11, a bio-sourced thermoplastic marketed as Rilsan® PA11 D30 NAT (Arkema, France), is derived from castor oil and consists of >90% renewable carbon (ASTM D6866). It has low water absorption (<1%) and a moderate melting temperature (189°C). The material was supplied in pellets for processing, with the specification shown in Table 1 and Figure 3(a).

BC particles (See Figure 3(b)) with a particle size of approximately 25 µm from a natural plant resource were provided as a raw particle-reinforcement material (Takesumi Ltd., Japan). It offers functional benefits such as flame retardancy, moisture regulation, and potential improvement in stiffness and energy dissipation when used as a reinforcement in polymer composites [26].

#### 2.2. Bio-composite filament preparation for FFF 3D printing

The flowchart in Figure 4 presents the process by which the bio-composites were produced. In the initial phase,

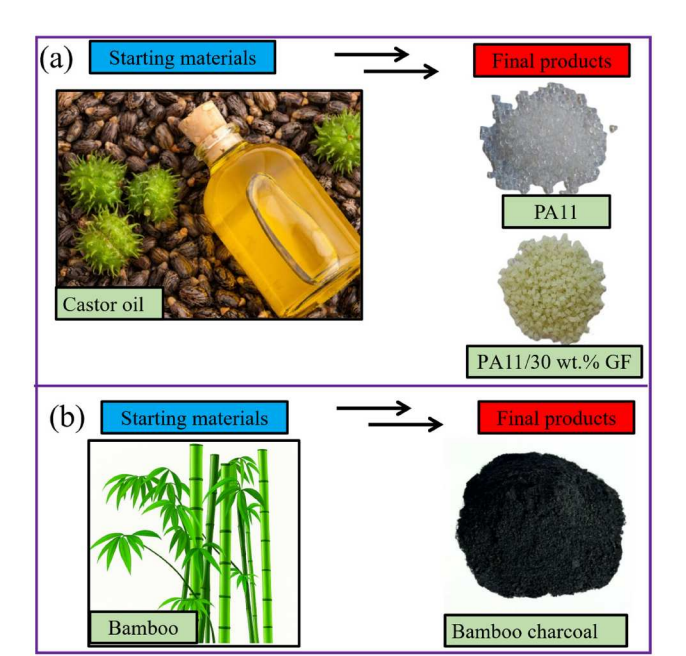


Figure 3. Composite compounds (a) PA11 and PA11/30 wt.% GF pellets, (b) BC powder.

Table 1. Selected data from PA11 and PA11/30 wt.% GF pellet datasheets.

		PA11/30 wt.%
Parameters	PA11	GF
Special Characteristics	Bio-based	Bio-based
Hardness, Shore D (COND)	68	74
Charpy notched impact strength (–30°C, Cond), kJ/m <sup>2</sup>	10.5	17
Flexural modulus (COND), MPa	1114	5560
Melt volume flow rate (MVR), cm <sup>3</sup> /10 min	30	9
Melting temperature (DSC @ 10°C/min),°C	189	189
Heat deflection temperature (1.8 MPa),°C	50	75
Specific gravity (23°C), g/cm <sup>3</sup>	1.03	1.25

pristine bio-based PA11 and glass-filled PA11 (30 wt.% GF) pellets were subjected to a drying regimen in a laboratory oven at 80°C for 12 h to eliminate residual moisture. Initially, the base materials, PA11 and PA11/30 wt.% GF pellets, as well as BC particles with varying weight percentages of BC (0, 1, 2, 3, 4, and 5 wt.%), were procured. The production of the bio-composite went through three distinct sequential steps: (1) PA11 and PA11/30 wt.% GF pellets and BC powder using a planetary ball mill at an operating frequency of 30 Hz. It uses 12 hard chromium steel balls with a 10 mm diameter and 5 same metal balls with a 15 mm diameter and has a ball-to-powder mass ratio of 1:2 in a steel vial with a volume of 150 ml. Composites were milled and blended at a rotational speed of 100 rev/min for 10 min to ensure a homogeneous distribution. (2) Composite filament extrusion, which was performed using a Filabot EX2, USA equipped with a speed-controlled spooler. The extrusion temperature was fixed at 180-190°C, and the screw speed was fixed at 30 rpm to, producing bio-composite filaments of consistent 1.75 ± 0.05 mm diameter. (3) 3D printing was carried out using an FFF-based 3D printer (Original Prusa MK4S). While optimisation of printing parameters could be insightful, but it is out of the scope of the present study and could be systematically investigated in future endeavour. Therefore, the set of FFF printing parameters including the nozzle temperature, was kept constant for all formulations to ensure stable processing conditions and allow a fair comparison among different composite systems. The printing parameters are listed in Table 2. PA11 bio-composites filaments and those reinforced with varying weight percentages of BC are denoted as PA11/X wt.% BC, where X indicates 0, 1, 2, 3, 4, and 5.

#### 2.3. Material characterisation

#### 2.3.1. Investigation of warping deformation

Warpage is one of the major unresolved challenges in AM, particularly in FFF, where it significantly limits the

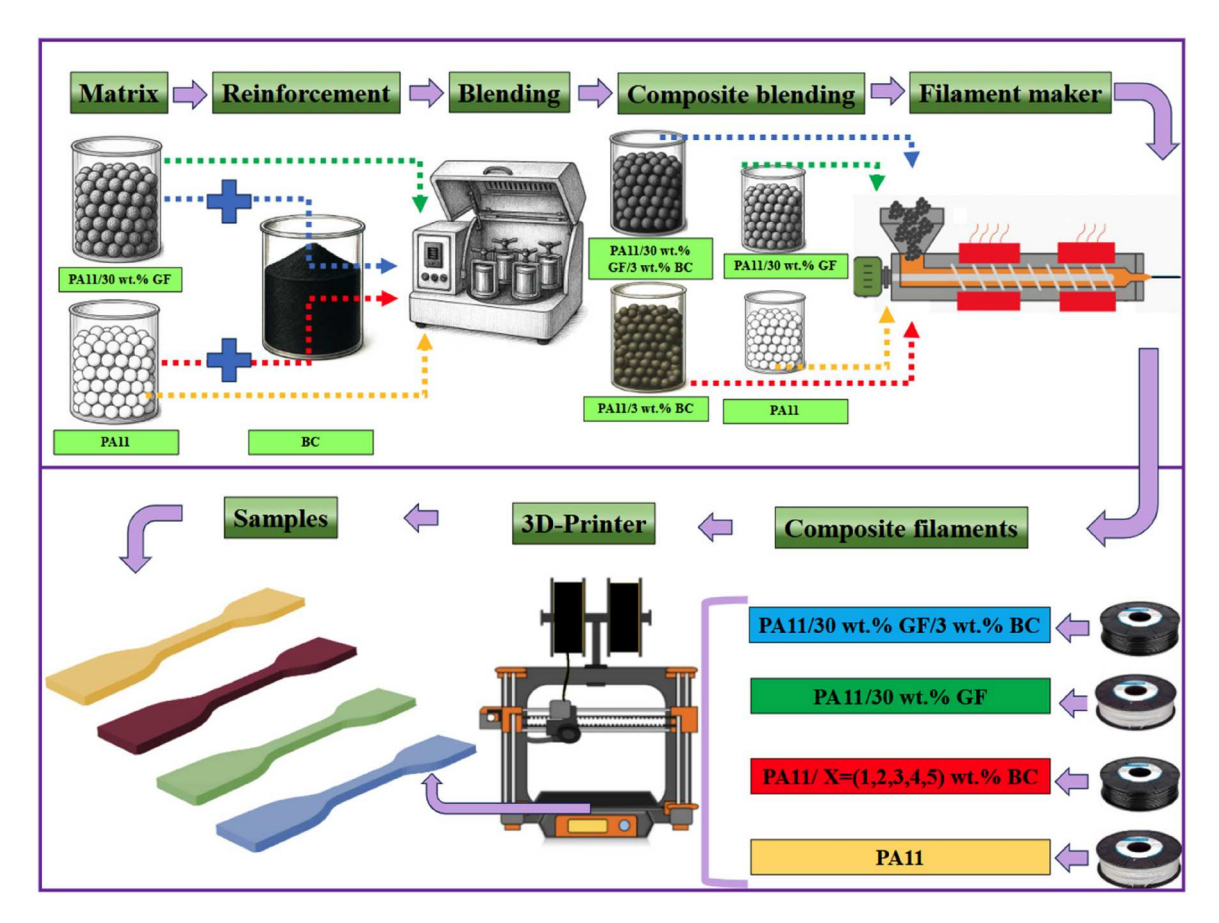


Figure 4. A detailed schematic of the fabrication of bio-composites from preparation to fabrication involving mixing raw PA11 and PA11/30 wt.% GF and BC particles, filament extrusion, and 3D printing of PA11 bio-composites to generate testing samples.

dimensional accuracy and industrial applicability of 3Dprinted parts. In this study, to evaluate warping deformation, five specimens were printed for each composition, and the specimen edges were measured immediately after printing using feeler gauges and high-precision callipers. Measurements were taken at all four corners and at the midpoint of each edge, and the average values and standard deviations were calculated to ensure statistical reliability of the reported data.

#### 2.3.2. Microstructural evaluation

Scanning electron microscopy (SEM) was employed to examine microstructural analysis to assess the BC and

Table 2. 3D printing parameters for the fabrication of biocomposites.

Parameters	Value
Nozzle diameter (mm)	0.4
Layer thickness (mm)	0.3
Printing speed (mm/s)	80
Infill density (%)	100
Printing pattern	Linear
Nozzle temperature (°C)	245
Bed temperature (°C)	90

GF distribution and the fracture surfaces to understand the bonding between PA11, BC, and GF. A JSM-7100F LV FEG machine was employed for this purpose. Before imaging, the samples were gold sputter coated with a 5 nm layer to enhance image clarity.

#### 2.3.3. Water contact angle measurement (WCA)

Surface energy and wettability/hydrophobicity are important characteristics in various applications of polymers including polyamides that come into regular contact with fluids, including in the automotive industry. For example, in engine compartments, it ensures resistance to moisture and oil; also, in interior consoles, it underpins adhesion of paints and coatings. Thus, it helps improve the durability and performance of automotive polymer components. Wettability testing was conducted on the novel PA11 biocomposites using an optical tensiometer (Theta Lite). A material sample was placed on the testing bed, and a water drop with a volume of 5 µL was introduced onto its surface via an injector. Meanwhile, a CCD camera captured the data, which was subsequently processed using the One Attention software package.

#### 2.3.4. Dynamic mechanical thermal analysis (DMTA)

A DMTA machine (DMA 8000, PerkinElmer) was utilised to investigate the thermo-mechanical behaviours in the 3D-printed specimens. Bio-composites were tested in the bending mode using a cantilever beam. Before testing, all specimens were conditioned at 35°C for 48 h. The DMTA testing procedure consisted of a temperature ramp from 25°C to 100°C at a rate of 2°C/min. Storage modulus and tan  $\delta$  versus temperature were calculated throughout the test procedure.

#### 2.3.5. Flammability evaluation

The flammability properties of the bio-composites were analysed to evaluate the resistance of composite materials to flame propagation in interior components of different industries, including the automotive sector, for applications such as dashboards, door panels, and centre console panels, using an Underwriters' Laboratories (UL-94) method. The flammability was assessed in accordance with ASTM D635-22 and ASTM D3801, respectively, to measure the burning rate and duration in a horizontal position and limiting oxygen index (LOI) measurements, and cone calorimeter tests (CCTs) in a vertical position [27]. Horizontally and vertically mounted 3D-printed samples were placed in a fume hood and marked at 25 and 100 mm from one end.

#### 2.3.6. Mechanical properties

Tensile tests were conducted on each different bio-composite at different temperatures, according to the ASTM D638-02 standard. All specimens tested were type V specimens. A Shimadzu AG-X plus machine apparatus was utilised for the tensile tests. The elongation speed was set to 5 mm/min. Room conditions were preserved during the tests, with a 23°C temperature and 50% RH (ambient laboratory conditions). Flexural tests were also conducted in the same apparatus by replacing the tensile grips with a three-point bending module. Flexural tests were conducted according to the ASTM D790-10 standard. 3D printed specimens were dimensioned according to Figure 5, and the support span was set to 52 mm. Flexural loading rate was set to 5 mm/min, at ambient laboratory conditions.

#### 2.3.7. Micro-hardness measurements

The microhardness measurements were conducted according to the ASTM D2240 standard with the 35° truncated-cone indenter. The applied force was set to 150 g, and the indentation time was set to 10 s. The hardness of samples was measured using an analogue durometer, Sauter HB model HBA 100-0, manufactured by Sauter GmbH. Indentations were performed on the polished surfaces of the fabricated specimens.

#### 2.3.8. Impact tests

Impact tests were carried out following the ASTM D6110-04 standard. Bio-composites were dimensioned according to Figure 5. An Izod's impact apparatus (Tec Equipment Ltd., UK) was employed in the tests.

In this study, all mechanical tests were carried out on five specimens per group under ambient laboratory conditions, without any prior conditioning, and results are reported as means ± standard deviations. All samples were 3D printed along their longitudinal axis, as can be seen by the blue and red arrows in Figure 5. Also, Figure 5 presents the ASTM-standard 2D drawings alongside photographs of the 3D-printed specimens (with magnified positions) and summarises the printing directions, specimen dimensions, and indicates tensile, flexural, and impact test samples.

#### 3. Results and discussion

#### 3.1. Investigation of warping deformation

Warp deformation, a geometric defect particularly common when printing semi-crystalline polymers such as PA11, arises from non-uniform thermal shrinkage during cooling. As the bottom layers cool and contract faster than the top layers, residual stresses build up, causing edge lift, distortion from the build plate, poor interlayer adhesion, and ultimately undesirable part geometries [28]. Common solutions include enhancing substrate adhesion with ridges or rafts, controlling the build environment via uniformly heated chambers, and selecting materials with lower shrinkage to improve dimensional stability, have been widely reported in the literature [29,30].

This study proposes a novel strategy with added reinforcements to decrease warping in FFF and validate its effectiveness by measuring warp deformation (see Figure 6). PA11 was reinforced with BC and GF via melt-blown filament extrusion, and then the resulting deflections and warp heights were measured. For each composition, five replicates were measured, and the average values ± standard deviation are reported. As shown in Figure 6, unreinforced PA11 exhibited an average corner lift of  $3.81 \pm 0.12$  mm (measured with a digital calliper). Incorporating 3 wt.% BC reduced this lift to  $2.58 \pm 0.09$  mm, due to decreased volumetric shrinkage and enhanced heat dissipation from the bamboo. A bio-composite blend of 3 wt.% BC and 30 wt.% GF effectively eliminated visible warping (0.1 ± 0.12 mm corner lift, measured with a feeler gauge),

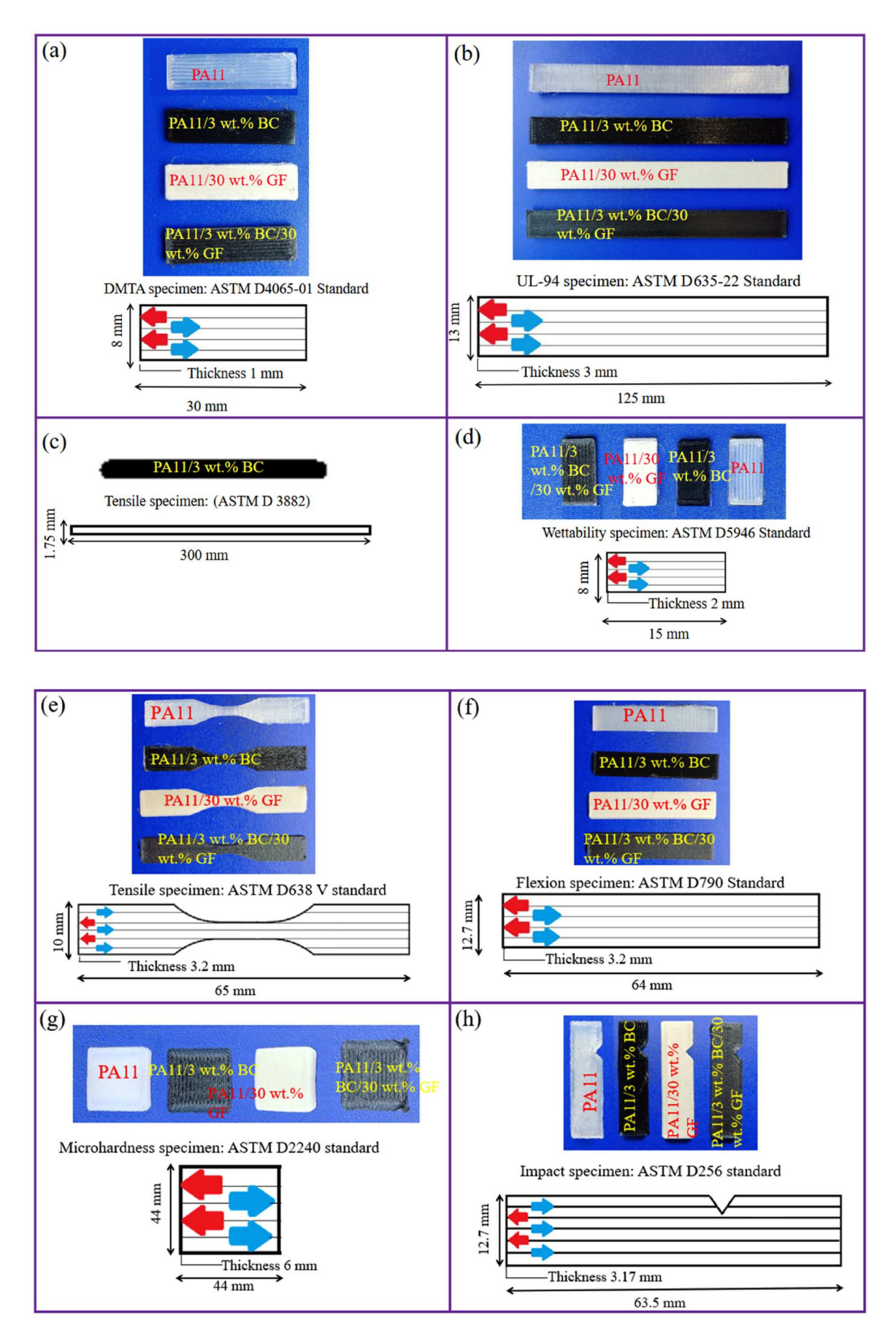
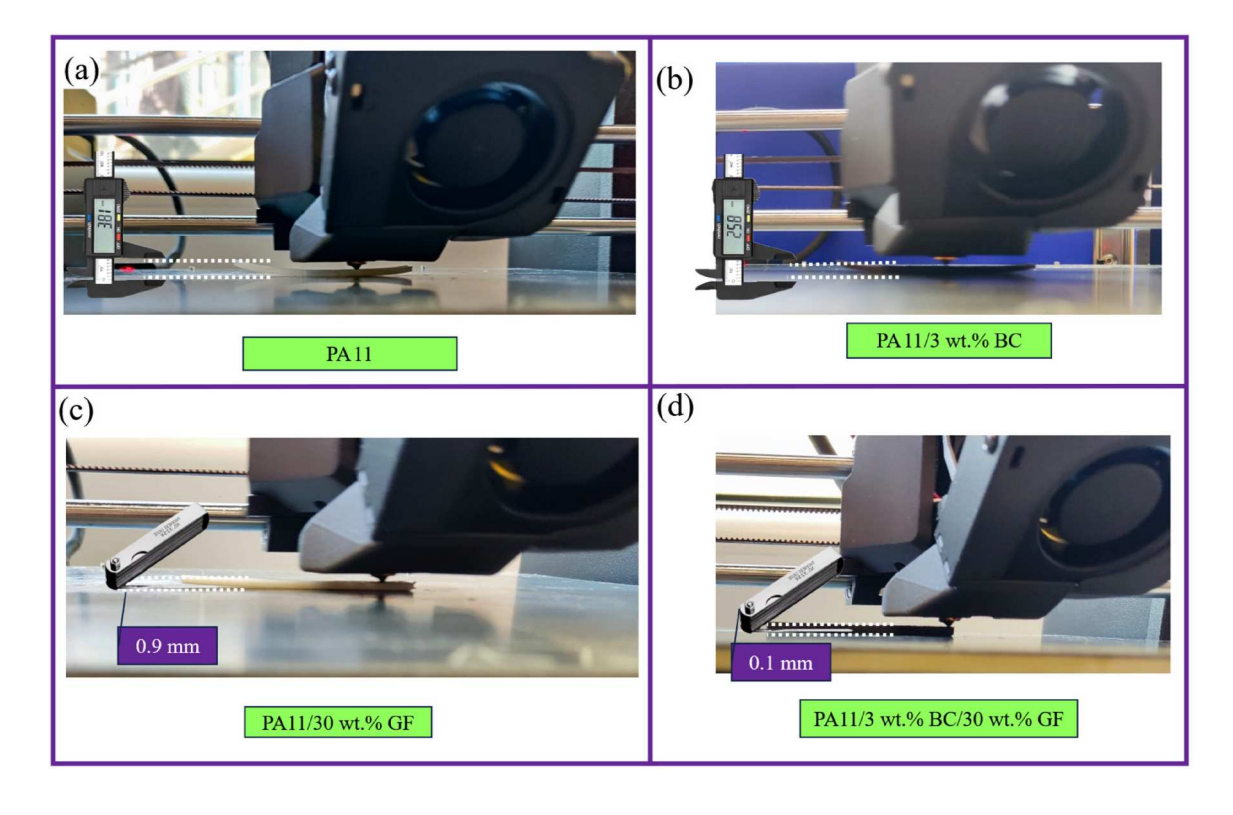
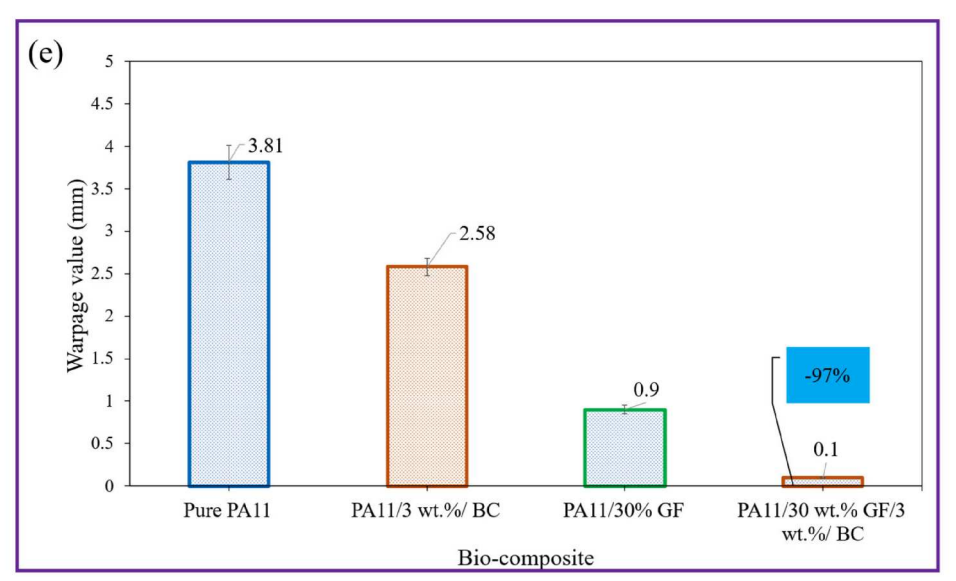


Figure 5. Images of the 3D-printed PA11 bio-composites designed according to ASTM standard, along with the testing method (a) DMTA, (b) UL-94, (c) tensile test (bio-composites filaments), (d) wettability, (e) tensile test (printed bio-composites), (f) flexion test, (g) micro hardness, (h) impact test.





**Figure 6.** Effect of BC and GF reinforcement on warpage measured using calliper and feeler gauge of (a) PA11, (b) PA11/3 wt.% BC, (c) PA11/30 wt.% GF, (d) PA11/30 wt.% GF/3 wt.% BC, (e) comparison of warpage measurement in PA11 bio-composites.

resulting in a 97% decrease compared to PA11. This is due to the fact that GF and BC provide thermal insulation and slow cooling, thereby lowering internal stress. In this research, to ensure consistency of the samples, a specialised adhesive was applied to the printer bed to prevent residual distortion, thereby ensuring that all samples were produced without visible warp defects.

Notably, PA11 can also warp in injection moulding since crystallization in this semi-crystalline polymer

causes non-uniform shrinkage when cooling is uneven has been previously studied and documented [31,32]. Non-uniform shrinkage and uneven cooling, along with fibre orientation in reinforced grades, can cause parts to warp after ejection and fall outside flatness tolerances, particularly in large flat areas or regions with thickness variations. In contrast, FFF printing of materials reinforced with glass fibres and bamboo charcoal reduces differential shrinkage and thermal stresses,

resulting in 3D-printed reinforced specimens with minimal warpage.

#### 3.2. Microstructure study

Figure 7 presents SEM micrographs of the fracture crosssections of PA11 and PA11 bio-composites (original Figure 7 image is shown in the supplementary material). In PA11 (Figure 7(a)), the fracture surface appears smooth and homogeneous, with no discernible voids, providing a clear baseline morphology. With the addition of 3 wt.% BC (Figure 7(b)), BC particles are dispersed within the PA11 matrix and exhibit clean, well-bonded interfaces, thereby increasing the effective interfacial area for stress transfer. In the PA11/ 30 wt.% GF composite (Figure 7(c)), GF (average diameter  $\approx$  8.2 µm) are oriented mainly parallel to the fracture plane. The fibres are well embedded in the matrix, although localised matrix - fibre debonding is evident and act as a crack-initiation barrier under tensile loading. These fibres serve as the primary load-bearing phase, markedly increasing stiffness and strength. The bio-composite (3 wt.% BC + 30 wt.% GF; Figure 7(d)) exhibits a synergistic microstructure: (1) BC particles

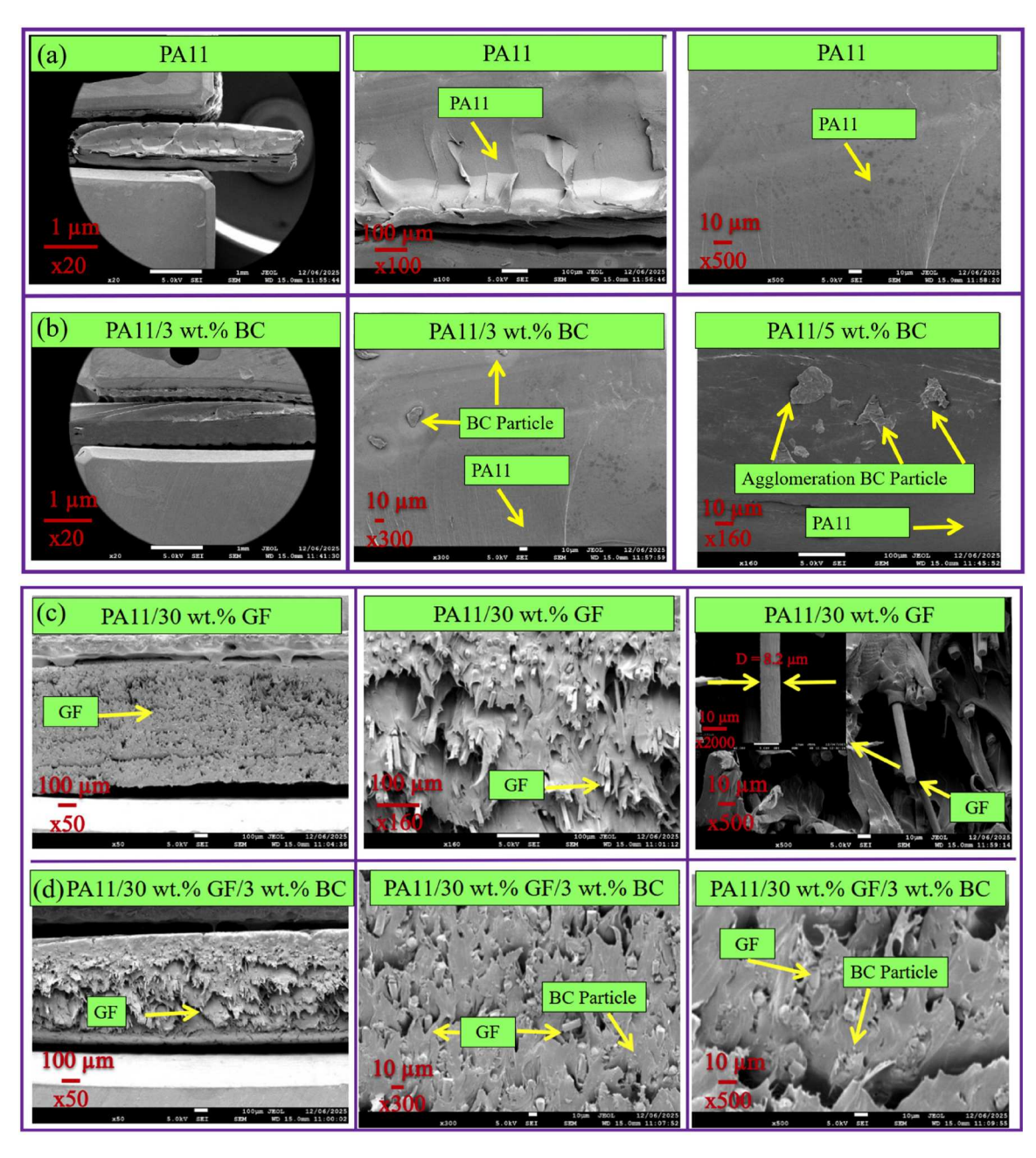


Figure 7. Cross-sectional SEM micrographs at different magnifications of (a) PA11, (b) PA11/3 wt.% BC, (c) PA11/30 wt.% GF, (d) PA11/ 30 wt.% GF/3 wt.% BC.

occupy the interstices among the glass fibres, (2) both reinforcements show strong interfacial adhesion to the PA11 matrix, (3) fibres and particles appear well contained, consistent with improved stress transfer and reduced propensity for crack growth.

#### 3.3. Wettability characteristics

I. WCA testing directly quantifies a material's surface wettability and its tendency to absorb or repel liquids under service conditions. Figure 8(a-f) shows the evolution of WCA from the initial angle (A°) to the final angle (B°) over 10 s for PA11 and bio-composites. PA11 begins at 62.25° and decreases steadily to 57.7°, reflecting higher surface polarity and rapid wetting. Adding 3 wt.% BC raises the initial mean angle to 69.6° and stabilises at 69°, indicating reduced surface energy. With 30 wt.% GF, the initial mean angle reaches 72.1° and stabilises at 71.9°. The PA11/3 wt.% BC/30 wt.% GF bio-composite shows the highest and most stable WCAs (78.17° initially, 77.49° at 10 s), with an improvement of 34% compared to PA11, demonstrating the strongest resistance to wetting (i.e. hydrophobicity) among all bio-composites.

Figure 8(g) summarises the mean angle values of A° and B°, confirming that both reinforcements, especially in combination, significantly increase hydrophobicity and suppress dynamic contact-angle decay. A higher, more stable contact angle (see appearance of water droplets) indicates lower surface energy and improved resistance to fluid ingress, fuel-tank condensation, and environmental attack. PA11 reinforced with BC and GF exhibits enhanced, durable hydrophobicity and therefore supports the development of bio-composite parts that meet modern vehicle durability and safety requirements.

#### 3.4. DMTA

Figure 9 shows the evolution of the storage modulus (E') and  $\tan \delta$  of PA11 and its bio-composites as a function of temperature. The measured glass transition temperature  $(T_q)$ , obtained from the tan  $\delta$  curves, is 52.1, 56.4, 59.3,

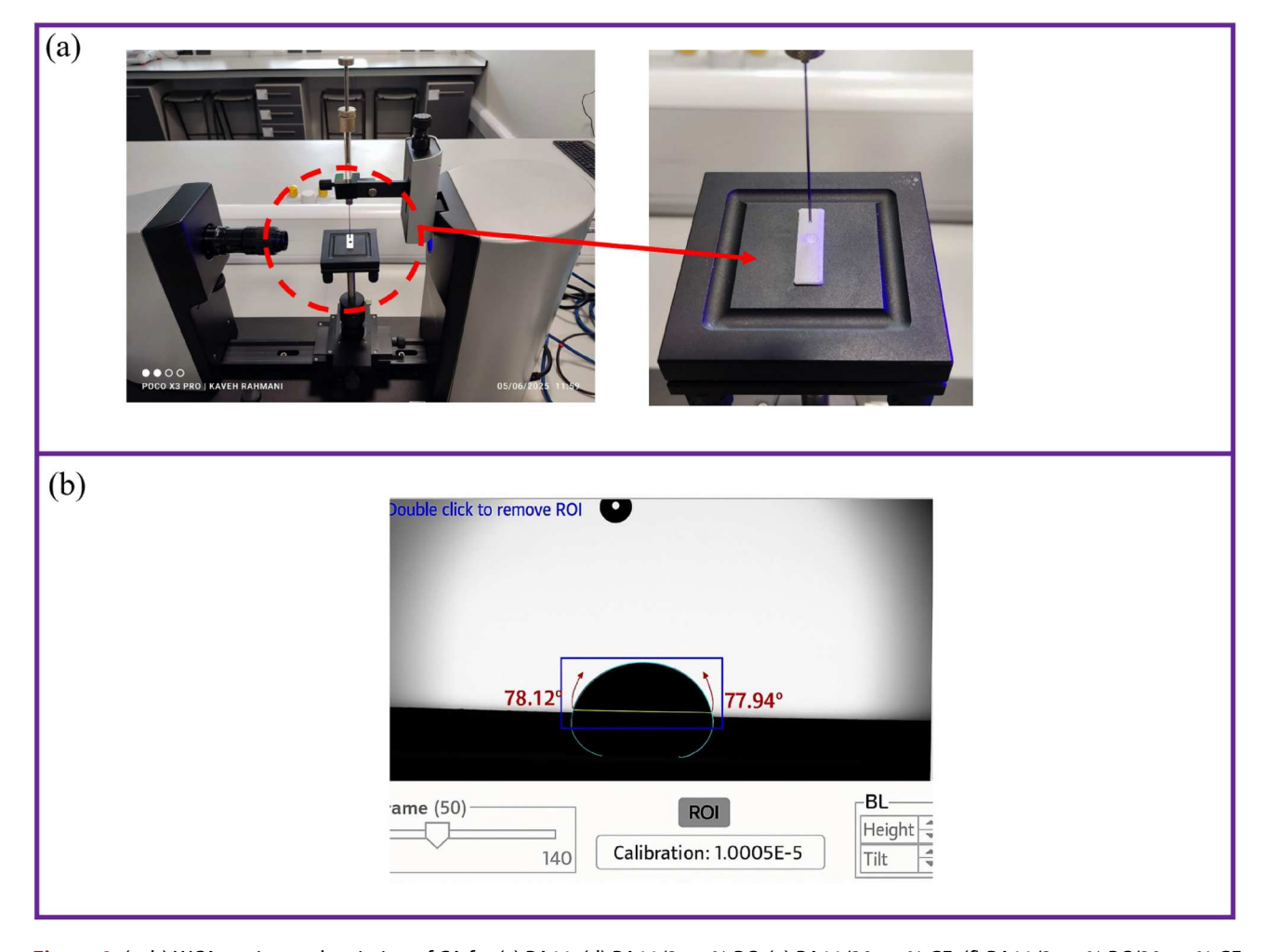


Figure 8. (a, b) WCA testing and variation of CA for (c) PA11, (d) PA11/3 wt.% BC, (e) PA11/30 wt.% GF, (f) PA11/3 wt.% BC/30 wt.% GF; and (g) compares of graphs of WCA mean.

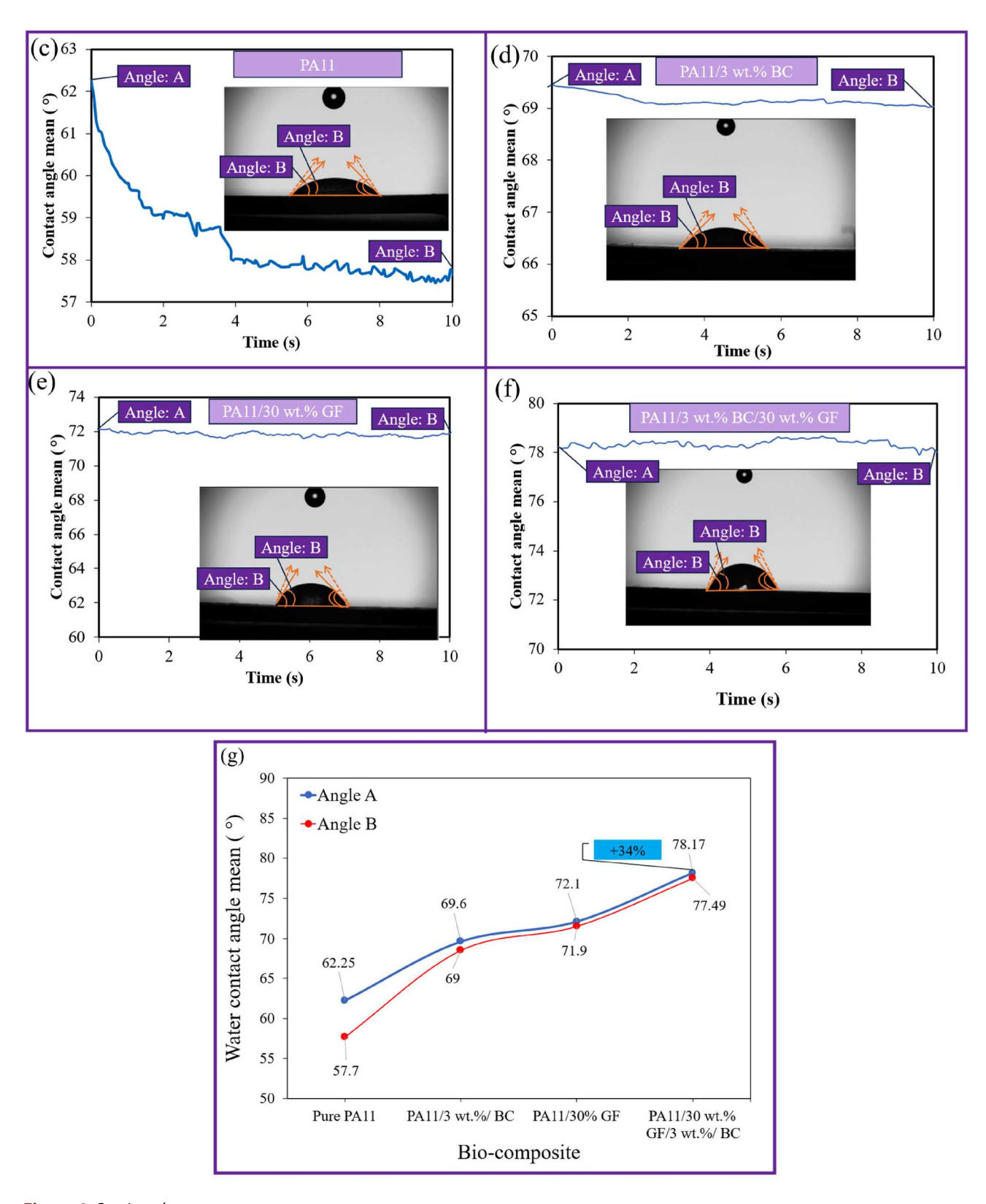
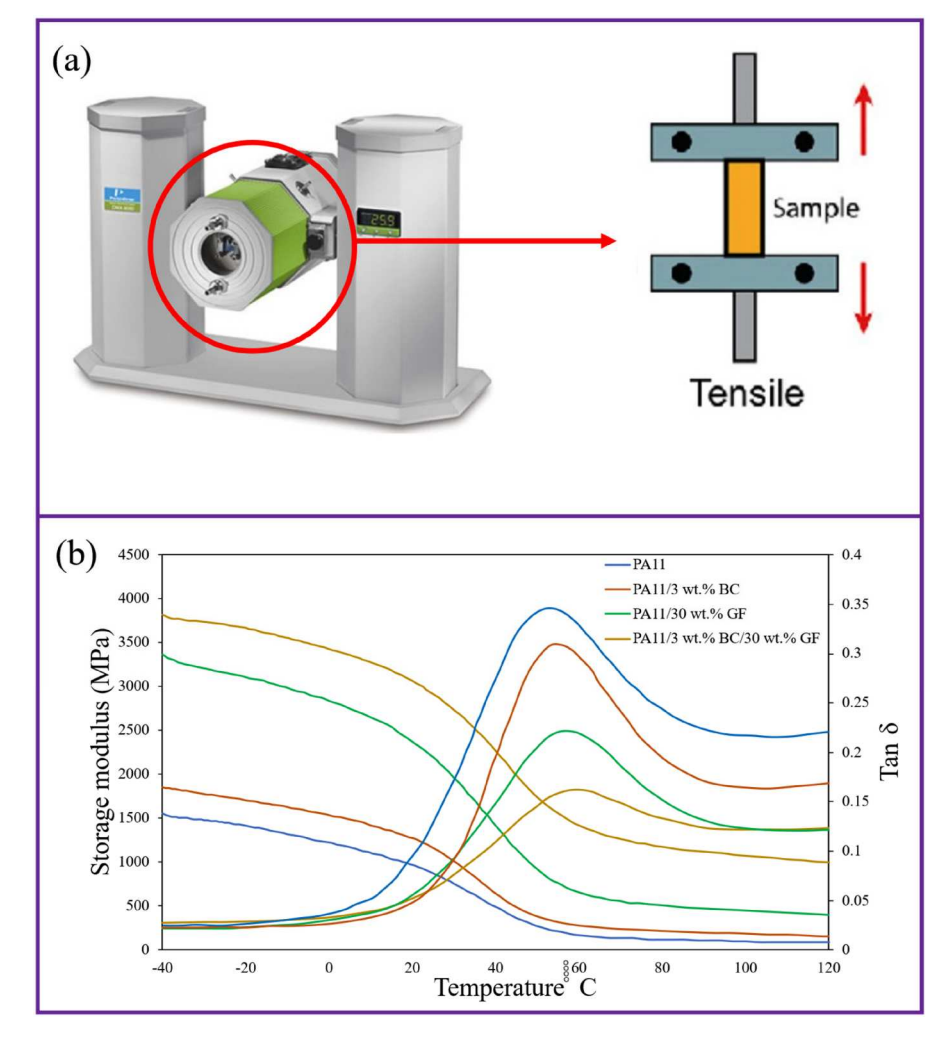


Figure 8 Continued

and 62.2°C for PA11, PA11/3 wt.% BC, PA11/30 wt.% GF, and PA11/30 wt.% GF/3 wt.% BC, respectively. Figure 9 indicates that  $\tan \delta$  decreases with increasing reinforcement content, as a consequence of the enhancement of

the storage modulus. As expected, higher storage modulus values were obtained for the composite materials due to the stiffening effect of the reinforcing materials [33]. For all samples, a slight decrease in



**Figure 9.** DMTA results of PA11 and PA11 bio-composites, (a) device for test (b) storage modulus and tan  $\delta$  results.

storage modulus is observed when the temperature increased up to 20°C, resulting from a slight mobility gain in the polymer chains, followed by a significant drop once  $T_q$  was exceeded. Above  $T_q$ , the storage modulus values became very low, indicating high mobility of the polymer molecules in the PA11 phase. However, the presence of GF increased the stiffness of the material, maintaining higher storage modulus values due to the inherent stiffness of glass fibres, and partially preventing the modulus reduction beyond T<sub>a</sub>.

It is worth noting that the presence of fibres in the composite significantly reduced the mobility of the polymer chains at temperatures above T<sub>q</sub>. The influence of GF is clearly evident in Figure 9, where the storage modulus of PA11/30 wt.% GF/3 wt.% BC remains higher than that of PA11 with increasing temperature.

#### 3.5. Flammability properties

The bio-composite samples were subjected to the UL-94 horizontal burning test, as shown in Figure 10(a). Figure

10(b) indicates that among the tested samples, PA11/30 wt.% GF/3 wt.% BC, PA11/30 wt.% GF, and PA11/3 wt.% BC exhibited burning rate reductions of 61.9%, 27%, and 12%, respectively, compared to PA11. This reduction in burning rate can be attributed to several factors. The presence of GF and BC particles forms insulative (char) layers that inhibit the penetration of heat and volatile substances into the composite, leading to lower burning rates and incomplete combustion compared to PA11. The addition of GF and BC enhances flame retardancy by reducing the material's overall flammability and dripping [34]. Figure 10(c-f) shows the samples before testing, during combustion, and after burning. This research highlights the potential of GF-reinforced PA11 with bio-derived bamboo-charcoal additives to produce flexible and fire-resistant materials for diverse applications, including automotive fire-safety standards, thereby helping to reduce fire-related damage in vehicle accidents.

The flammability of PA11 and its bio-composites was evaluated using UL-94, LOI, and cone CCT. The findings

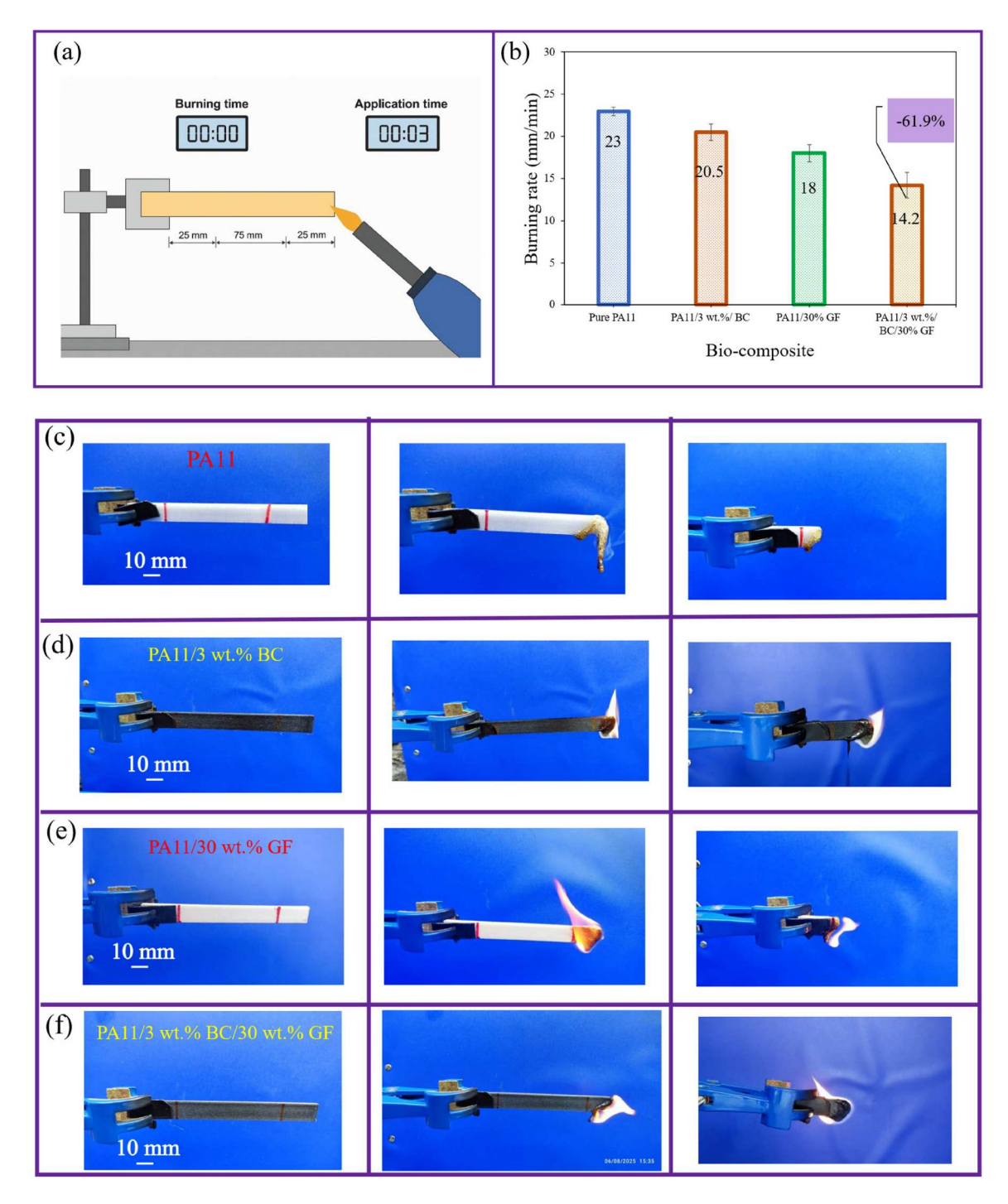


**Figure 10.** (a) Visual documentation of specimen clamping and ignition during the UL-94 horizontal burning test, (b) burning rates of PA11-based composites, (c-f) PA11 and bio-composites before testing, during combustion, and after burning.

are detailed in Table 3. The LOI results, expressed as the minimum oxygen concentration required to sustain combustion, showed that pure PA11 had an LOI of 23.2%. Incorporating BC slightly improved flame resistance, while the combined addition of GF and BC produced higher LOI values. The PA11/3 wt.% BC/30 wt.% GF bio-composite achieved the highest LOI of 29.1%, mainly due to the formation of a compact char layer acting as a thermal and physical barrier that limits

**Table 3.** UL-94, LOI and CCT results for PA11 and PA11 biocomposite.

UL-94 (Vertical)							
Samples	Dripping	Rating	LOI (vol.%)	pHHR (kW/ m <sup>2</sup> )	TTI (s)		
PA11 PA11/3 wt.% BC PA11/30 wt.% GF PA11/3 wt.% BC/30 wt.% GF	Yes Yes Yes Yes	NC* NC NC V2	23.2 24.9 26.6 29.1	973 829 721 654	49 40 37 31		

<sup>\*</sup> No Classification (NC)

oxygen diffusion and heat transfer. Moreover, the UL-94 rating of PA11 improved from 'No Classification' to V-2 with the addition of BC and GF.

The cone calorimeter test results further confirmed these improvements. The peak heat release rate (pHRR) values of PA11/3 wt.% BC/30 wt.% GF, PA11/30 wt.%GF, and PA11/3 wt.% BC decreased by 35%, 25%, and 14%, respectively, compared to pure PA11, indicating improved fire performance. The incorporation of BC and GF also delayed the time to ignition (TTI) due to the formation of a continuous char network that restricted heat flow. However, BC alone slightly reduced the TTI of PA11 because it promotes heat absorption and earlier degradation. In contrast, GF enhanced structural stability, reduced dripping, and extended the burning time, demonstrating a synergistic improvement in the overall flame retardancy of the composites [34].

#### 3.6. Mechanical properties

#### 3.6.1. Tensile properties of PA11-BC composites

The tensile strength behaviour of 3D-printed bio-composites fabricated from PA11 reinforced with BC powder at weight percentages of 0, 1, 2, 3, 4, and 5% was evaluated in accordance with ASTM D638-Type I standards (illustrated in Figure 11). The experimental results showed that incorporating 3 wt.% BC powder into PA11 produced the maximum improvement,

28.3 MPa, in ultimate tensile strength (UTS) among all tested compositions. Based on these findings, 3 wt.% BC was identified as the optimal reinforcement level, and all later mechanical evaluations in this study were conducted using this composition. It can be concluded that for reinforcement contents above 3 wt.%, the tensile properties of both the filaments and the 3Dprinted specimens no longer improved, as higher reinforcement loadings failed to induce any additional reinforcement effect. In fact, excessive reinforcement content may cause a reduction in the mechanical properties of the bio-composites, likely caused by BC particle agglomeration, which can lead to stress concentration under mechanical loading [26,35]. To validate the regarding reinforcement agglomeration at higher filler content, SEM analysis was conducted on PA11 bio-composite. As shown in Figure 7(b), the PA11/3 wt.% BC composite exhibit a relatively uniform dispersion of particles, while the PA11/5 wt.% BC sample clearly reveals visible agglomerates and clustering of BC particles.

## 3.6.2. Tensile properties of PA11 and PA11 biocomposites

Tensile tests were performed for the PA11 and the biocomposite filaments at the first stage (Figure 12), as well as on 3D-printed coupons in the second stage (Figure 13). Figure 12(a) shows a polymer filament under testing, while Figure 12(b) demonstrates the tensile strength of bio-composite filament under quasi-

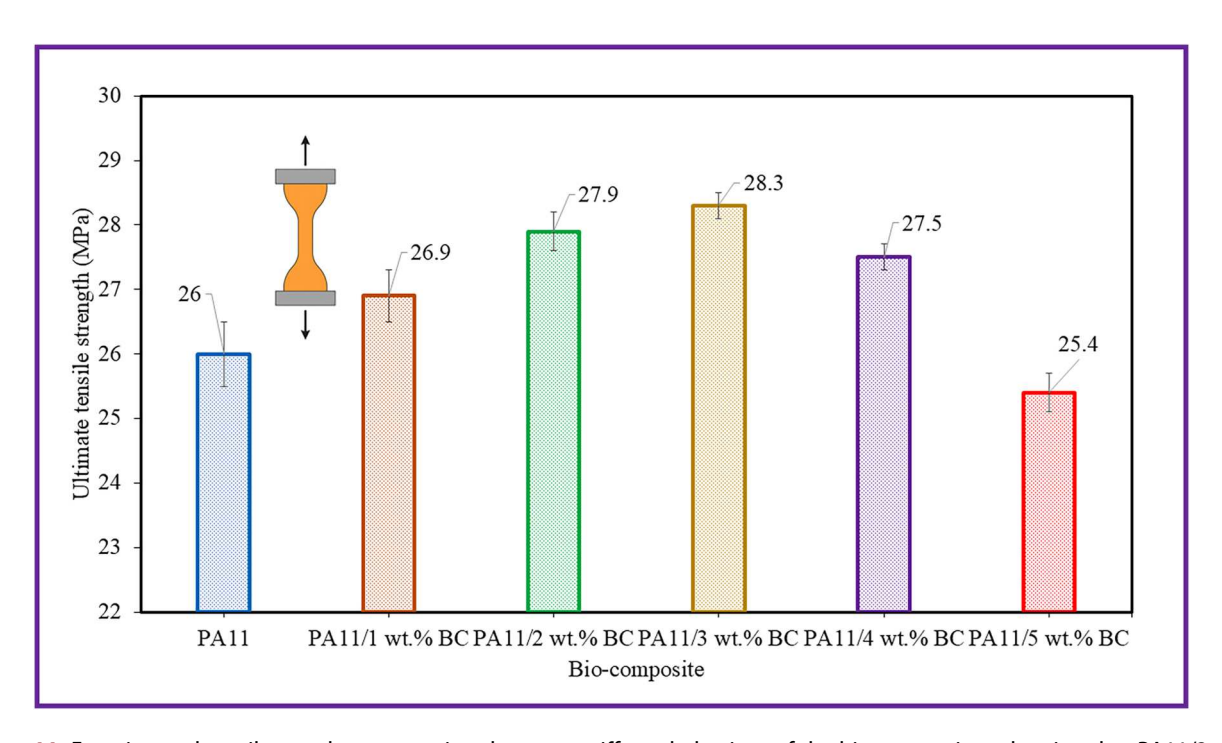


**Figure 11.** Experimental tensile test data comparing the stress-stiffness behaviour of the bio-composites, showing that PA11/3 wt.% BC exhibits greater stiffness than other alternatives.

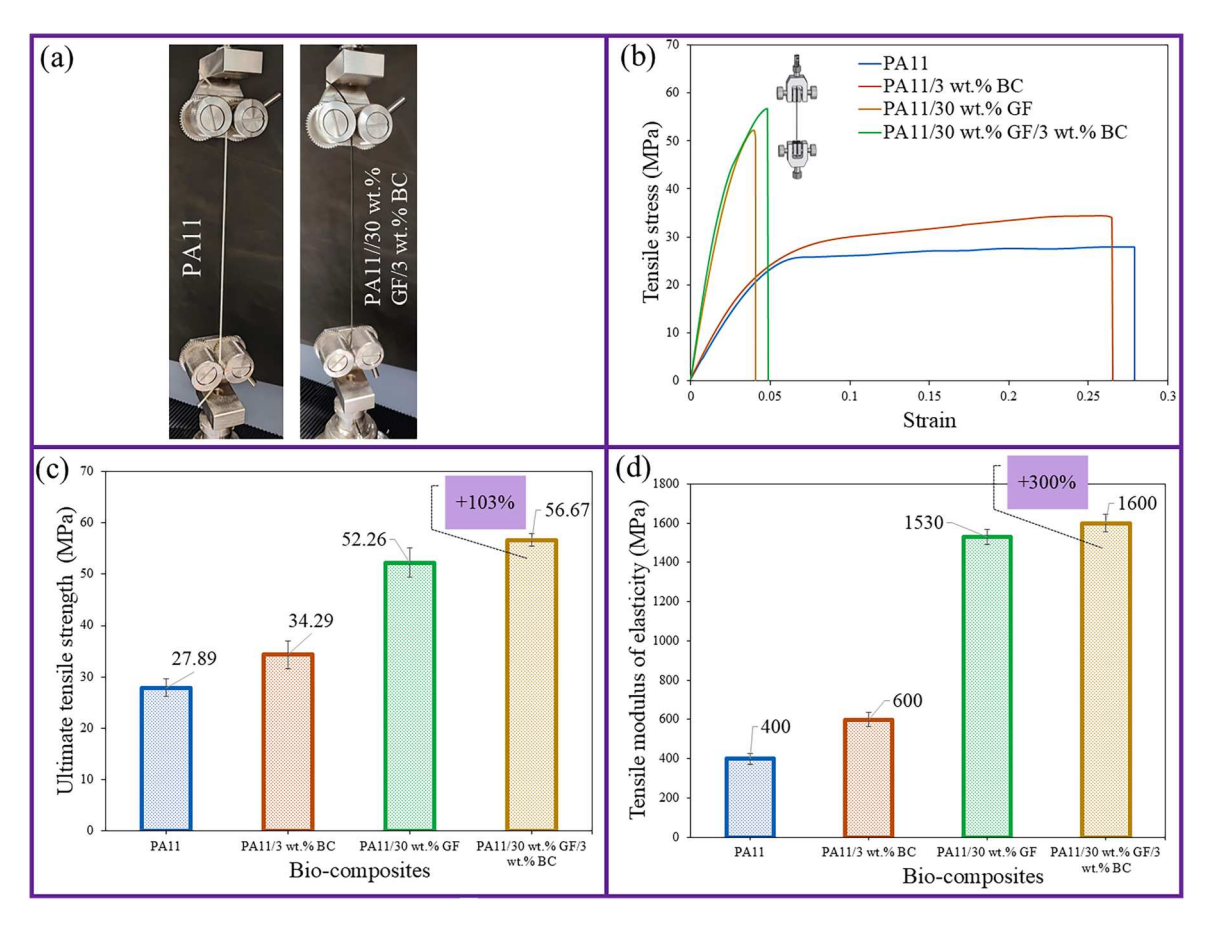


**Figure 12.** (a) Image of PA11 and PA11 bio-composite filaments under tensile testing, (b)stress-strain curve under tensile test, (c, d) UTS and tensile modulus of elasticity for 3D-printed PA11 and all bio-composite filaments.

static tensile loading. In Figures 12(c and d), the UTS and the modulus of elasticity properties are summarised, respectively, for all the different extruded and produced filaments in this research work (mean values with the corresponding standard deviation). For extruded filaments, BC and GF had a positive reinforcement effect for the different reinforcements. Specifically, the highest increase was observed in UTS and the tensile modulus at PA11/30 wt.% GF/ 3 wt.% BC, respectively 103% and 300%.

Figure 13(a and b) show a 3D sample under tensile test and stress–strain curves for PA11 and its bio-composites. Consistent with the filament results, Figure 13(c and d) summarise the UTS and modulus of elasticity (mean ± SD) for all samples. Both BC and GF act as effective reinforcements. The highest increase was obtained for PA11/30 wt.% GF/3 wt.% BC, with increases of 194% in UTS and 361% in modulus compared to PA11. In this regard, studies have shown that natural reinforced bio-composites can improve mechanical performance in 3D printing [36,37]. These improvements increase from (i) the stiffness and aspect ratio of GF, which enable efficient load transfer from the PA11 matrix to the fibres; (ii) rigid BC micro-particles that stiffen the matrix and act as stress-transfer bridges

[26]. In bio-composites, BC also occupies the inter-fibre matrix and roughens the interface, improving fibre-matrix adhesion and reducing micro-voids; as a result, with the higher strength and modulus observed [38].

From the above analyses, it can be concluded that GF and BC exhibit a more marked reinforcement effect on the tensile strength and modulus of elasticity of PA11, both in the extruded filaments and in their relevant 3D-printed specimens. In this study, the mechanical properties of the extruded filaments were compared with those of 3D printed samples. The filament tests represent the intrinsic properties of the material, while the 3D printed samples tests reflect the effect of the printing process, including porosity, interfacial adhesion, and void formation. By comparing these two sets of results, it is possible to distinguish of their on the influence of the tensile strength. Comparison of Figures 12 and 13 reveals that the tensile strength of the PA11 filament and the PA11 filament reinforced with 3 wt.% BC is higher than that of the corresponding 3D-printed specimens with the same compositions.

The reduction in tensile strength for the 3D-printed specimens is more pronounced in the PA11 and PA11/3 wt.% BC filaments, which can be attributed to the higher

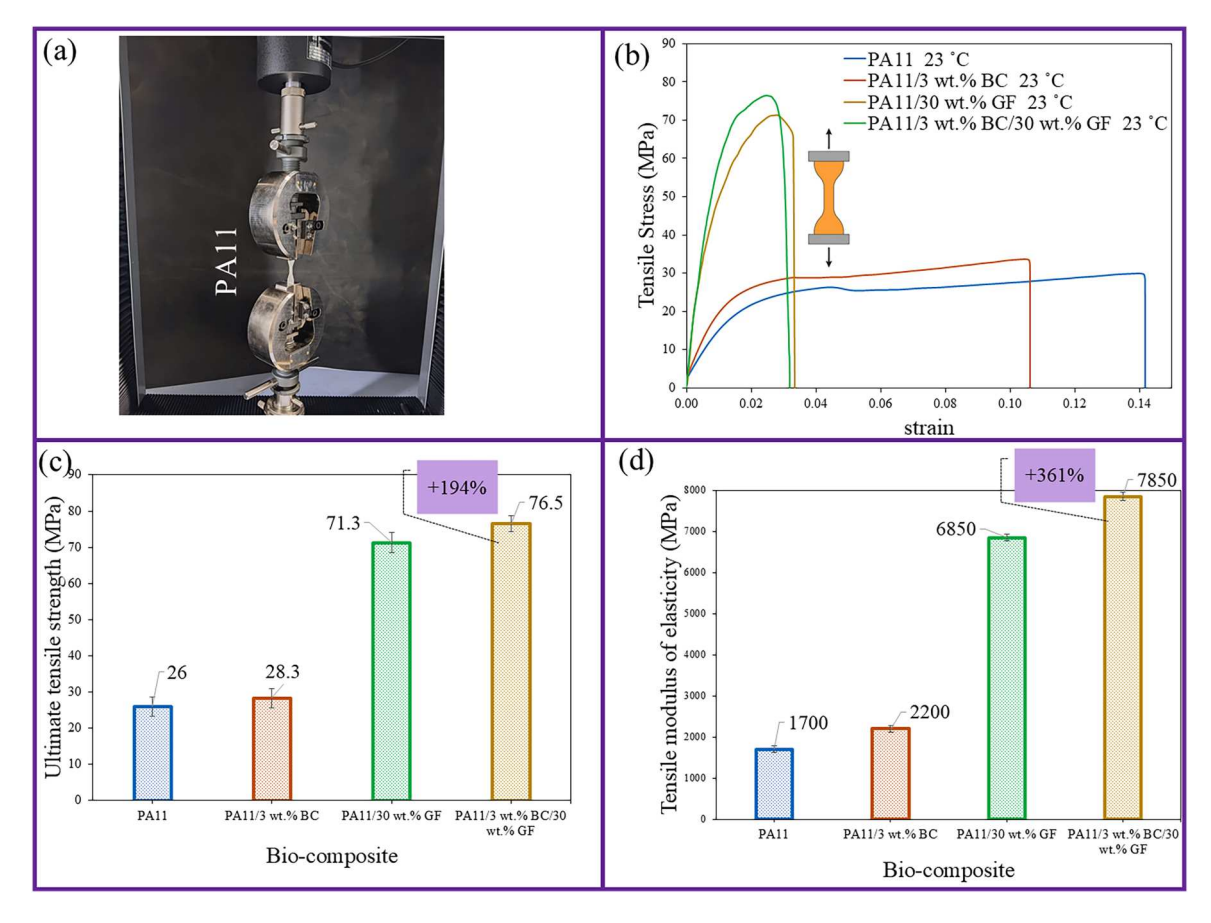


Figure 13. (a) Image of the sample under tensile testing, (b) stress-strain curves for PA11 and PA11 bio-composites, (c, d) tensile strength and tensile modulus of elasticity for PA11 and PA11 bio-composites.

void content in the printed samples compared to their corresponding single filaments. In contrast, when reinforced with 30 wt.% GF, both the 3D-printed PA11 and PA11/3 wt.% BC composites exhibited higher tensile strength than their respective single filaments. This improvement can be attributed to the enhanced fibre alignment and compaction along the printing direction, induced by the shear flow and pressure inside the nozzle during deposition. These conditions facilitate better fibre - matrix impregnation and stress transfer, thereby increasing the tensile strength of the printed composite. Additionally, the presence of BC particles may further promote interfacial bonding by forming a micro-network that restricts polymer chain mobility and enhances load-bearing efficiency. Two probable mechanisms for the mechanical reinforcement may include: (1) strong polymer matrix reinforcement interactions, and (2) a sufficient and highquality dispersion of particles within the polymer matrix.

#### 3.6.3. Tensile properties of PA11 and PA11 biocomposites at different temperatures

Polymers are used in a wide range of applications, but their mechanical properties can be significantly affected under high temperatures. Understanding their

performance in elevated temperatures is essential, as polymers exhibit varied responses that influence their reliability and functionality. The automotive industry is a prime example, where plastic components such as seals and connectors are exposed to varied temperature ranges throughout their service life. These temperature variations demand different material behaviours: at low temperatures, flexibility and impact resistance are required to prevent brittleness, whereas at elevated temperatures, dimensional stability and thermal resistance are crucial to avoid deformation. Recognising this thermal duality is fundamental for characterising the mechanical properties of polymers under realistic operating conditions.

This section focuses on the tensile test results of the bio-composites at elevated temperatures, highlighting the factors that influence their mechanical behaviour. High temperatures pose challenges to polymer resistance, often leading to changes in flexibility and stiffness, which are often characterised by properties including heat deflection temperature and Tg. Figure 14 presents the tensile stress-strain behaviour, UTS, and tensile modulus of PA11 and PA11 bio-composites tested at 50 and 90°C in a thermostatic chamber

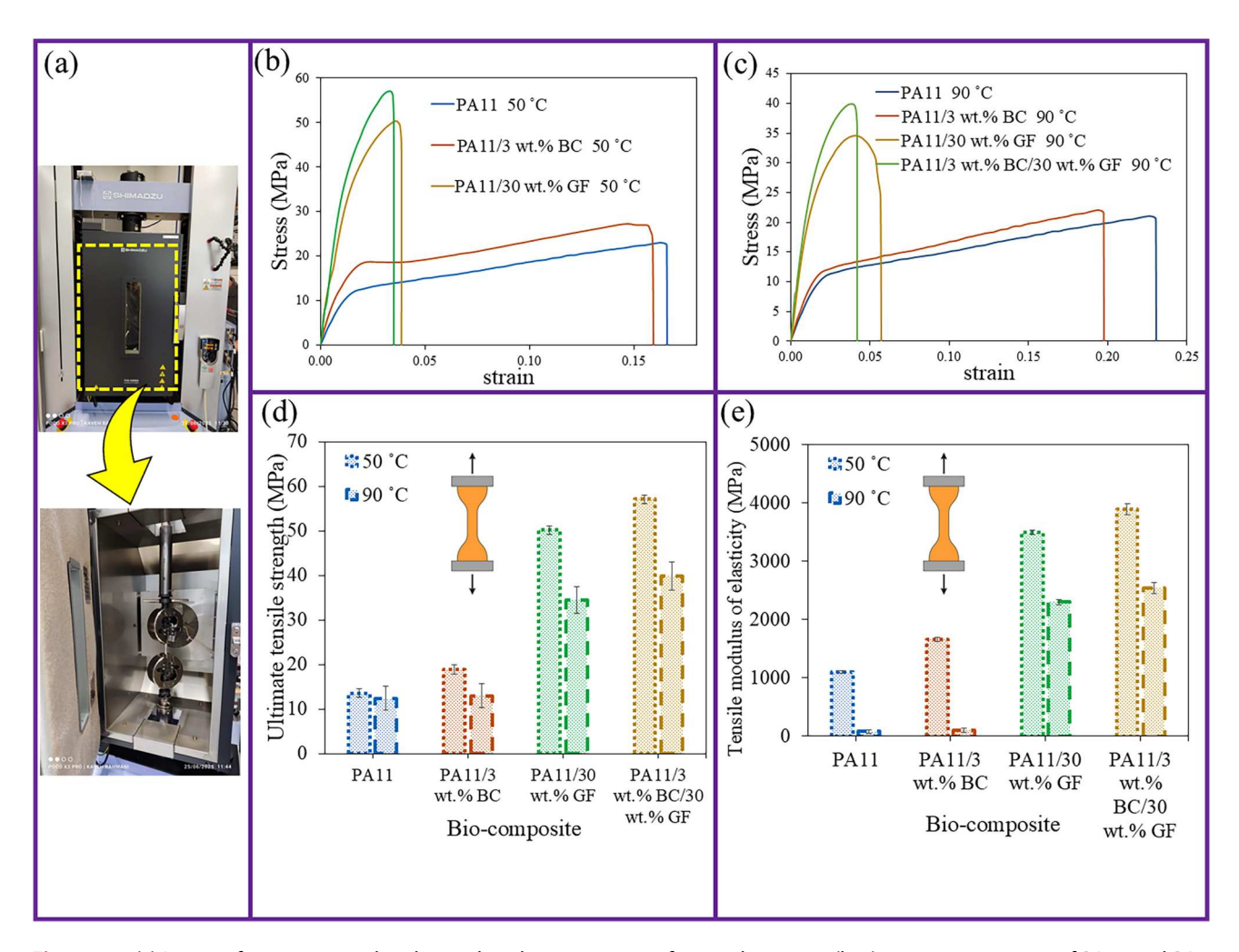


**Figure 14.** (a) Image of temperature chamber with a clamping system for tensile testing, (b, c) stress-strain curves of PA11 and PA11 bio-composites at 50, and 90°C, (d, e) UTS and tensile elasticity modulus of PA11 and PA11 bio-composites.

(Figure 14(a)). It was attached to the Shimadzu® AG-X universal testing machine, following ASTM D638 [8], with a prescribed speed of 5 mm/min. Figures 14(b and c) illustrate the influence of temperature on the mechanical response. The stress values decrease with increasing temperature due to enhanced Brownian molecular motion above the glass transition temperature [39]. This increased mobility of the polymer chains allows greater deformation, reducing the forces required for material strain. As a result of the higher degree of plasticisation, the failure strain increases, although in PA11/30 wt.% GF, this increase is limited by the constraining effect of the GF. However, the matrix softens, leading to a reduction in stress values.

At 50°C (Figure 14(b)), PA11 exhibits the lowest tensile strength and modulus, reflecting the inherent ductility of the non-reinforced polymer. The addition of 3 wt.% BC slightly increases both properties due to the stiffening effect of the particles and improved load transfer at the BC particle-matrix interface. Incorporating

30 wt.% GF results in a considerable increase in tensile strength and modulus, driven by the high stiffness and load-bearing capability of the GF. The PA11/3 wt.% BC/ 30 wt.% GF composition shows the highest performance, combining the reinforcing effects of both reinforcement and benefiting from a synergistic interaction. At 90°C (Figure 14(c)), all samples show reduced tensile strength and modulus due to softening of the PA11 matrix. However, the performance ranking remains with few changes, with the GF and hybrid composites keeping the maximum values, indicating better stability of mechanical properties at elevated temperatures. The UTS results in Figure 14(d) support these observations. At 50°C, the PA11/30 wt.% GF/3 wt.% BC sample achieves a value close to 57 MPa. At 90°C, strength decreases across all samples, but the GF-containing composites remain considerably stronger than PA11.

Similarly, the tensile modulus results (Figure 14(e)) show that at 50°C, the bio-composites, including GF

and GF/BC, reach values in the range of 1100-3900 MPa, several times higher than PA11. BC alone produces only a moderate increase. At 90°C, modulus values decrease, but the GF and GF/BC bio-composites still retain high stiffness, demonstrating their suitability for applications requiring dimensional stability under elevated temperatures. Overall, the results confirm that GF is the dominant contributor to stiffness and strength, BC provides additional toughening, and their combination makes a synergistic effect. Furthermore, GF and GF/BC bio-composites show high-temperature performance, making them strong candidates for structural applications in the automotive sector. It should be noted that a proper design of experiment along with statistical analysis could be carried out to decouple and quantitatively validate the individual and interactive contributions. However, it is out of scope of the current research and could be performed in future endeavour. One may refer to [40] for more details.

Figure 15(a) compares the tensile stress – strain curves of the bio-composites tested at 23, 50, and 90° C. As presented in Figures 15(b and c), the UTS and

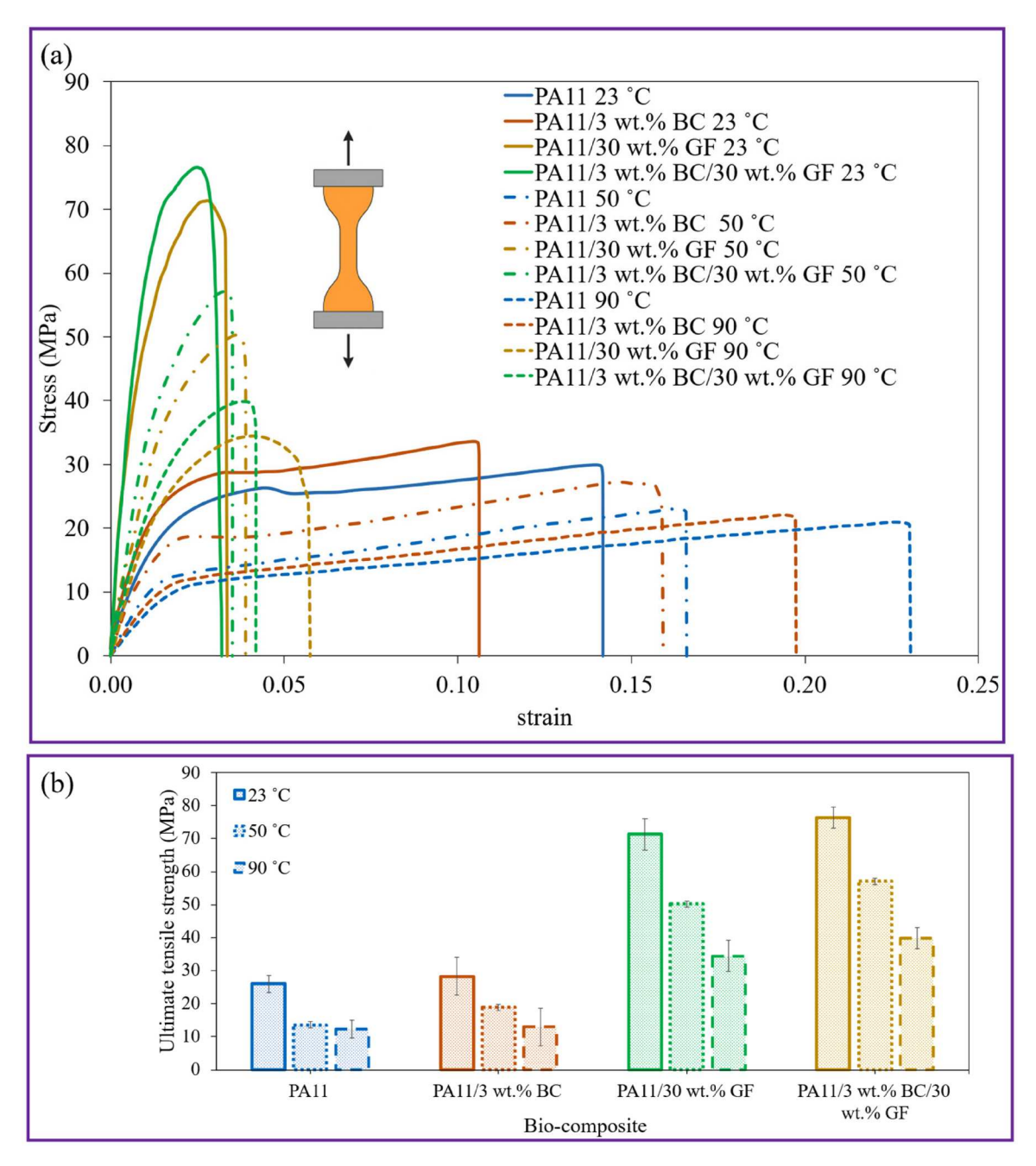


Figure 15. (a) Tensile test curves from 23°C to 90°C, (b, c) UTS and tensile modulus of elasticity of PA11 and PA11 bio-composites at 23, 50, and 90°C, (d) tensile modulus of elasticity at various temperatures.

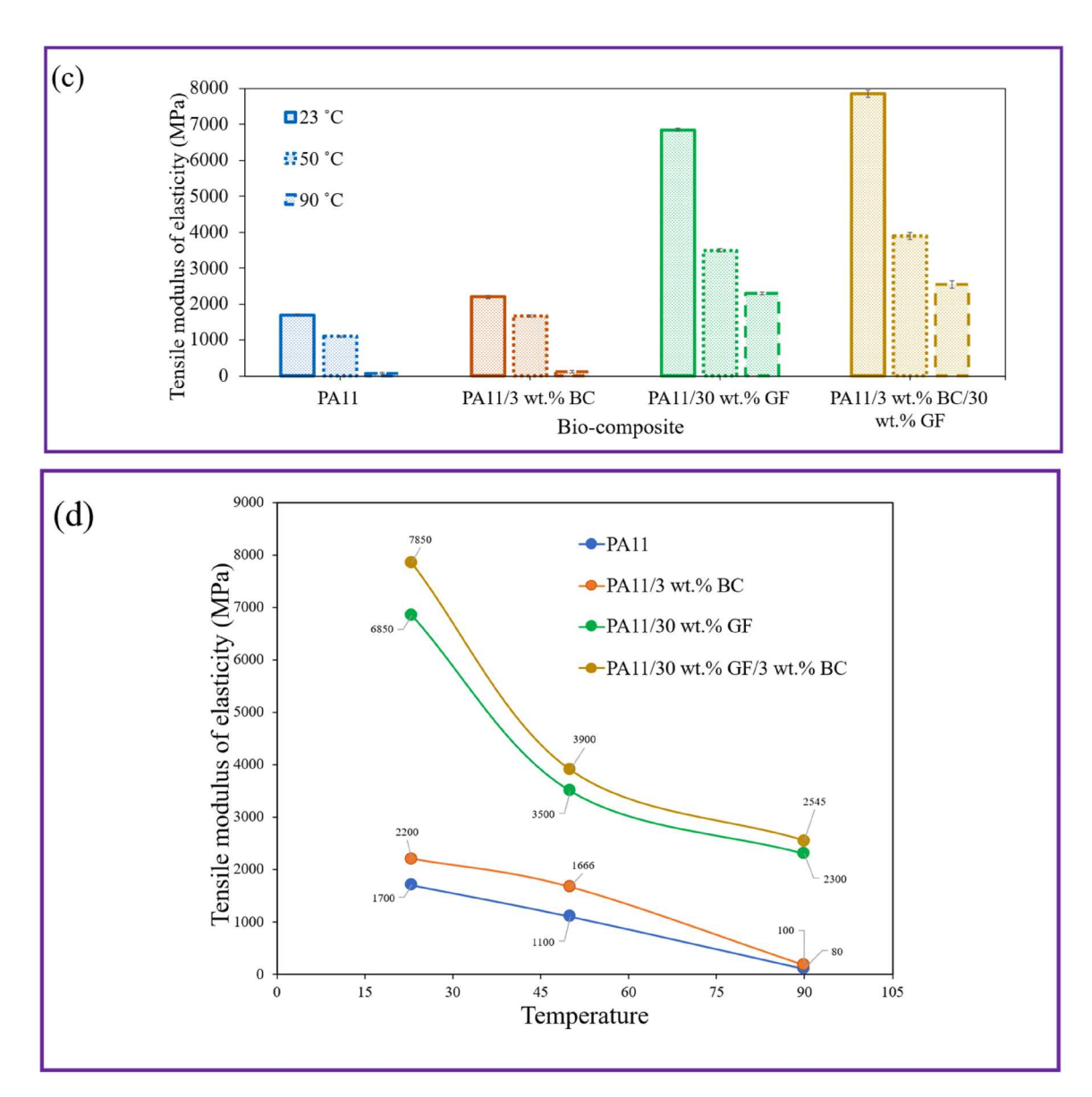
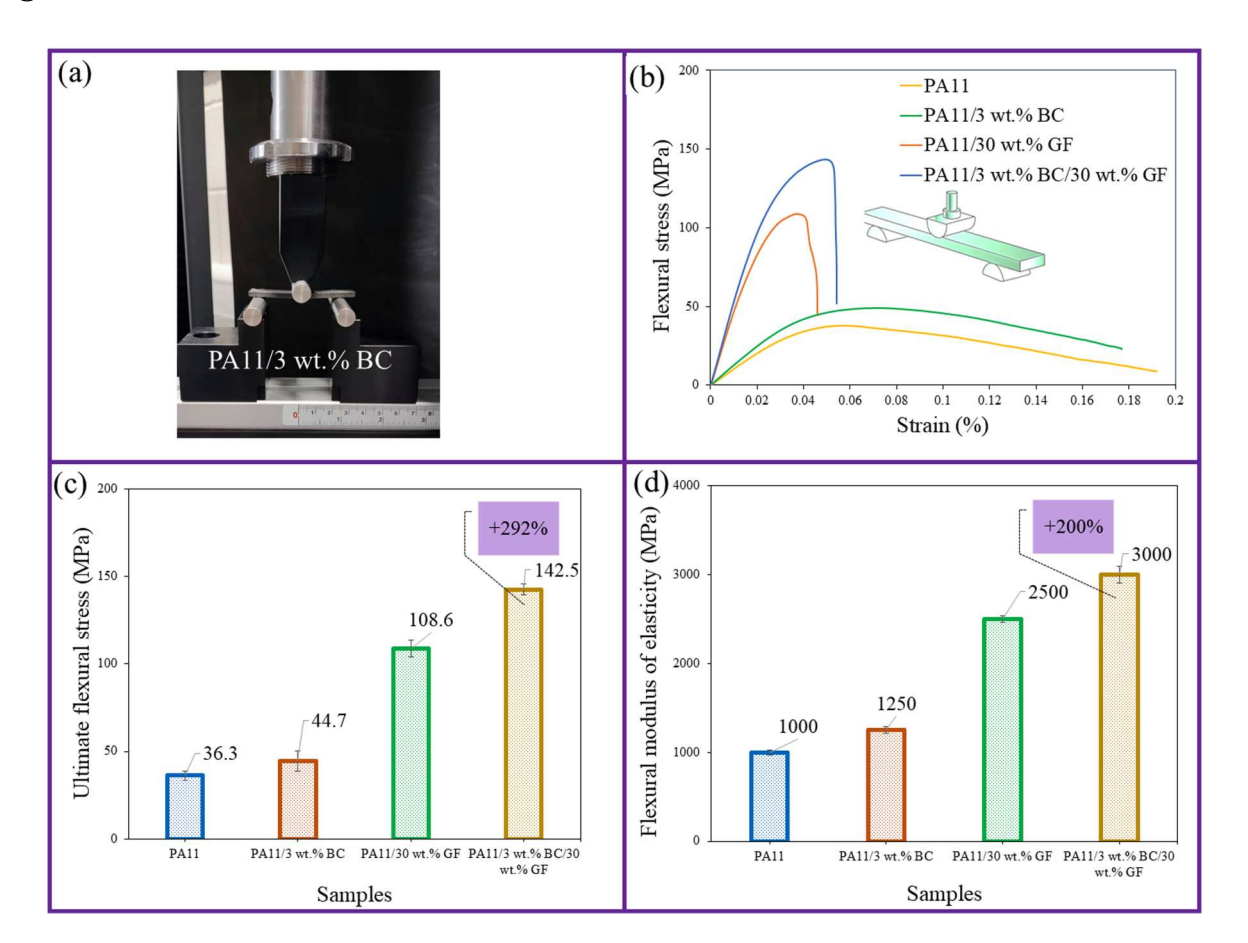


Figure 15 Continued

tensile modulus of all materials decrease steadily with increasing temperature. For the UTS in Figure 15(b), PA11 drops from 26 MPa at 23°C to 12.4 MPa at 90°C. BC-reinforced PA11 decreases from 28.3 MPa to 13 MPa, while GF-reinforced PA11 falls from 71.3 MPa to 34.5 MPa. The BC/GF hybrid starts at the highest value (76.5.5 MPa) and retains 39.8 MPa at 90°C, better performance than either of the singly-reinforced composites. Figure 15(c) compares the tensile modulus of PA11 and its bio-composites at 23, 50, and 90°C. At room temperature (23°C), PA11 has the lowest modulus (1.7 GPa), which increases slightly with BC addition (2.2 GPa), rises significantly with GF reinforcement (6.8 GPa), and reaches the highest value in the hybrid sample (7.85 GPa). As the temperature increases to 50° C, all materials soften: PA11 drops to 1.1 GPa, BC- reinforced to 1.67 GPa, GF-reinforced to 3.5 GPa, and the hybrid to 3.9 GPa. At 90°C, the modulus values converge at lower levels for PA11 at 0.08 GPa and BC-reinforced at 0.1 GPa, while GF and the hybrid retain much higher values of 2.3 and 2.55 GPa, respectively. The small error bars (±1 SD) confirm the consistency and repeatability of the measurements.

To better visualise the decrease in elastic modulus, Figure 15(d) presents a line plot showing the continuous decrease in tensile modulus for each composition as temperature increases from 23°C to 90°C. Overall, the results demonstrate that GF plays a dominant role in enhancing stiffness, BC provides modest improvements, and their combination achieves the highest mechanical performance and is maintained at all tested temperatures.



**Figure 16.** (a) Image of sample under flexure test, (b) stress-strain curves for PA11 and PA11 bio-composites, (c, d) tensile strength and tensile modulus of elasticity for PA11 and PA11 bio-composites.

# 3.6.4. Flexural test results of 3D-printed PA11 and PA11 bio-composites

Figure 16(a and b) present flexural testing and flexural stress–strain curves for the samples. The incorporation of BC alone produces a modest increase in stress, whereas GF significantly enhances both stress and the initial slope. The hybrid sample combines these effects, exhibiting the highest stress. Figure 16(c and d) quantify the average maximum flexural stress and the corresponding flexural modulus for each composition, including standard deviations. PA11 achieves a maximum flexural stress of 36.3 MPa and a modulus of 1 GPa. Incorporation of 3 wt.% BC increases the stress to 44.7 MPa and the modulus to 1.25 GPa. The 30 wt.% GF composite reaches 108.6 MPa and 2.5 GPa, while the BC/GF hybrid peaks at 142.5 MPa and 3 GPa, respectively.

These trends closely mirror the tensile results, confirming that BC primarily enhances stiffness, GF increases strength, and their combination produces a synergistic reinforcement effect in bending. Similar to the tensile behaviour, PA11/3 wt.% BC/30 wt.% GF shows a notable improvement in flexural properties, with the maximum flexural stress increasing by approximately

292% and the flexural modulus by about 200% compared to PA11.

## 3.6.5. Impact strength and micro-hardness properties

In industrial applications like automotive, components such as bumpers and interior panels must withstand impacts ranging from stone chips to crash loads. Impact energy-loss tests evaluate a material's ability to absorb and dissipate energy, reducing the likelihood of cracking. Figure 17 shows the average punch-energy-loss and Vickers microhardness (HV) values. The punch-energy-loss test (see Figure 17(a)) shows that impact resistance increases with reinforcement content (Figure 17(b)) [41]. PA11 dissipates 0.32 kJ/m², while adding 3 wt.% BC doubles this to 0.571 kJ/m². With 30 wt.% GF, the value rises to 1.05 kJ/m² due to the presence of fibres and strong bonding between fibre and matrix. The PA11/3 wt.% BC/30 wt.% GF reaches 1.74 kJ/m², showing a high synergistic effect.

Figure 17(c) indicates a sample under a hardness test, and Figure 17(d) illustrates improved Shore-A hardness with reinforcements. Pure PA11 measures 94 ShA, increasing to 98 ShA with 3 wt.% BC and 99 ShA with

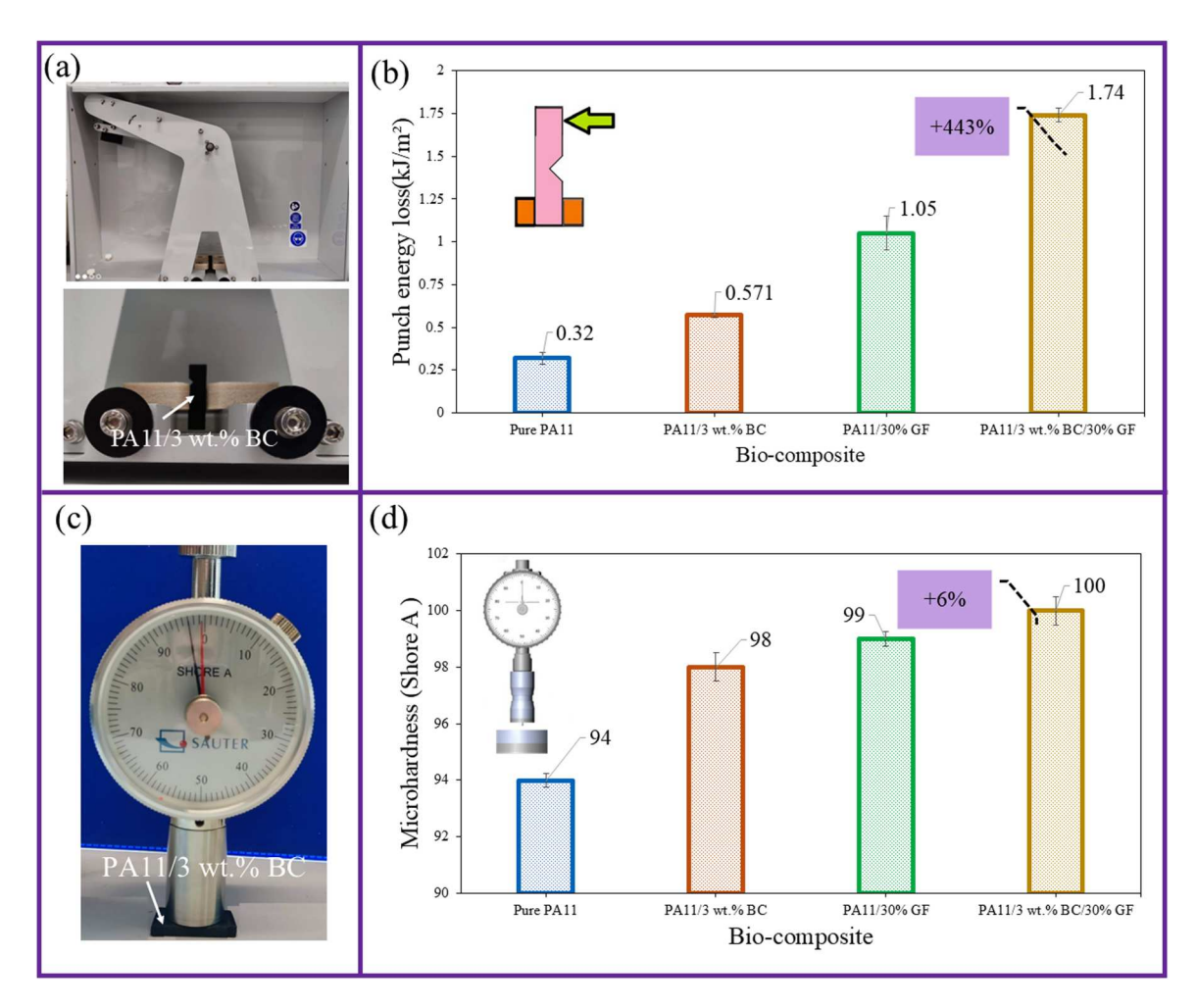


Figure 17. (a, b) The impact energy-loss test and its results; (c, d) the Shore A hardness test and its results for PA11 bio-composites.

30 wt.% GF. The 3 wt.% BC and 30 wt.% GF incorporated to PA11 reaches 100 ShA. These small hardness gains, along with the large increase in impact energy, indicate that reinforcements enhance stiffens without making the material brittle. According to the impact and hardness results, the PA11/30 wt.% GF with 3 wt.% BC biocomposite exhibited the best performance, with impact resistance and microhardness increasing by 443% and 6%, respectively, compared to PA11. These enhancements are attributed to crack-arrest mechanisms that enable the material to absorb more energy before failure [42]. The results of this research show that PA11 bio-composites reinforced with BC and GF are stiffer and absorb more impact energy, making them suitable for durable, safe automotive parts.

Figure 18 presents a radar (spider) chart summarising this study's results, including mechanical properties, impact-energy loss, Shore A hardness, and burning rate of PA11, PA11/3 wt.% BC, PA11/30 wt.% GF, and PA11/3 wt.% BC/30 wt.% GF. Across all axes, the PA11/3 wt.% BC/30 wt.% GF sample compared to PA11

shows the largest gains: at 23°C, tensile strength increases from 26 to 76.5 MPa (+194%), and tensile modulus from 1.7 to 7.85 GPa (+362%). Also, flexural strength nearly quadruples (36.3–142.5 MPa), and flexural modulus triples (1–3 GPa). Impact energy absorbed rises from 0.32 to 1.74 J, and Shore A hardness from 94 to 100, and the burning rate decreases from 23 to 14.2 mm/min, remaining within acceptable thresholds for automotive components. These results demonstrate that BC particles impart stiffness and help deflect cracks, GF supplies load transfer, and their combination produces a bio-composite with balanced, synergistic reinforcement.

#### 4. Bio-composite structures

Recent advances in multi-material additive manufacturing have enabled the fabrication of high-performance components that combine complementary material properties with architected geometries [28]. Multimaterial AM systems and design strategies, including

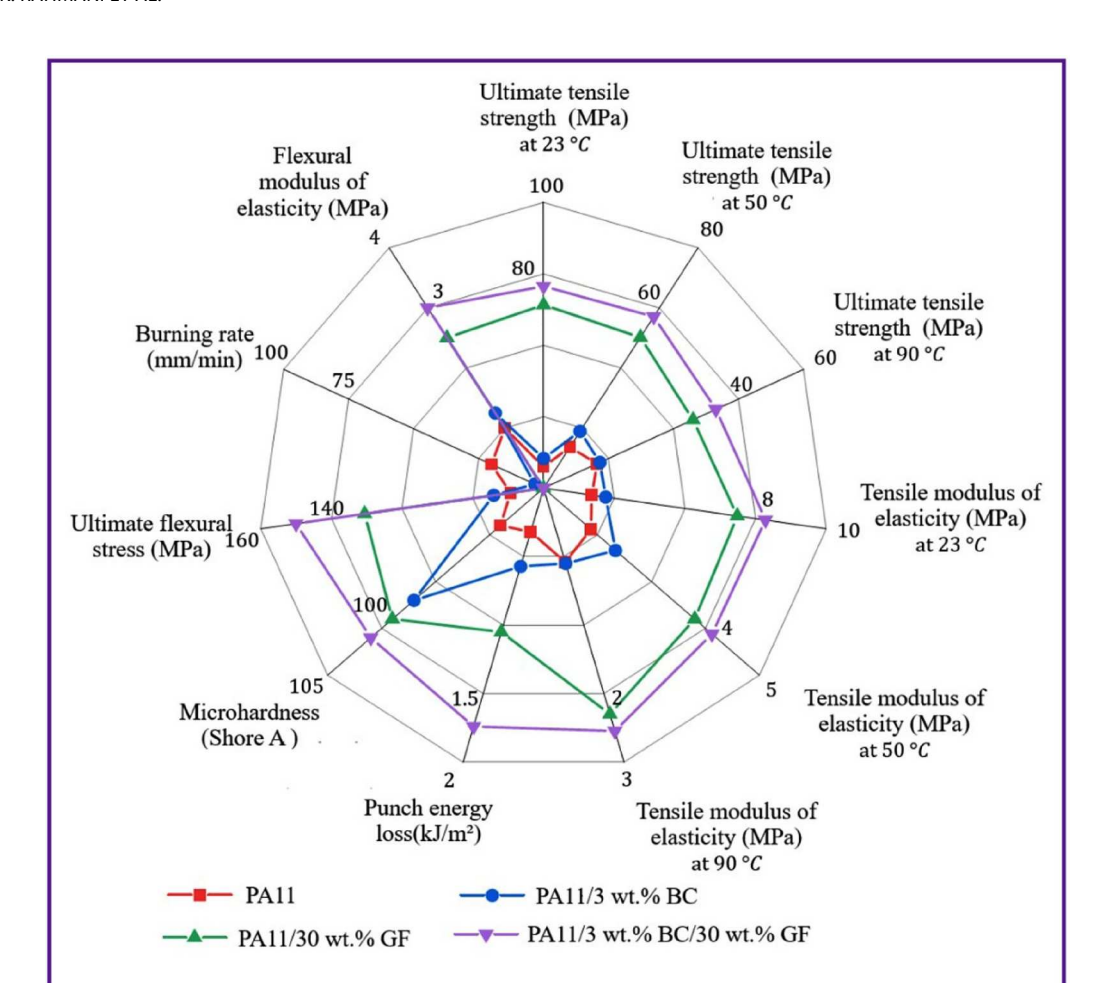
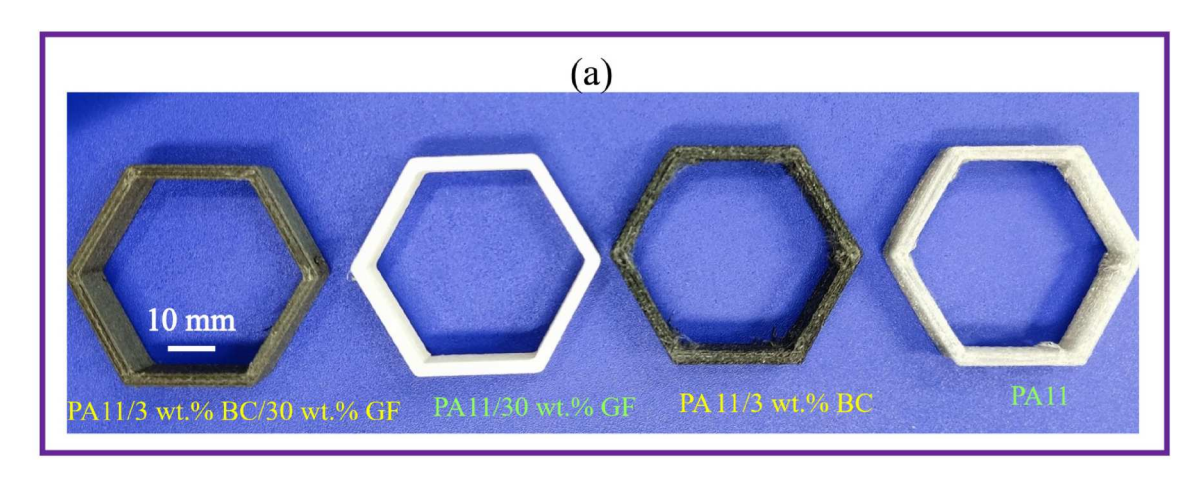


Figure 18. Spider chart summarising the experimentally determined tests of PA11 and PA11 bio-composites.

material gradients, hybrid material printing, and multimaterial lattice design, have been reviewed extensively and shown to help tailor local mechanical response and failure modes [43]. Cellular lattice topologies, particularly hexagonal/honeycomb variants, consistently demonstrate high specific strength and superior energy absorption-to-weight ratios compared with many conventional topologies. Design choices such as cell shape, relative density, and graded density strongly influence peak force, plateau stress, and total energy absorbed [44]. Several experimental and numerical studies report that combining multi-material approaches such as stiff/dense skins with compliant cores or hybrid polymer/metal lattices markedly improves crashworthiness and impact attenuation for automotive and motorsport applications, making AM lattices promising candidates for crash boxes, bumper elements, and protective gear [45]. There is also growing interest in bio-based and natural-fiberreinforced feedstocks (including bamboo-derived charcoal, flax, and other biomass fillers) for 3D printing. These materials enable lighter, more sustainable lattice

and composite designs while offering competitive mechanical and energy-absorbing performance when properly optimised.

In this study, honeycomb meta-bio-composite structures, as shown in Figure 19(a) were fabricated through 3D printing of PA11 and PA11 reinforced with BC and GF. Their mechanical performance was evaluated by loading and unloading at a constant crosshead speed of 5 mm/min. Each specimen, with an initial height of 40 mm, was compressed to displacements of 5 and 20 mm, corresponding to 12.5% and 50% compression, respectively. The deformation states at different compression levels are shown in Figures 19(b and c), while the corresponding force-displacement responses are provided in Figures 19(d and e). Figure 19(b) shows that PA11 and the meta-bio-composite reinforced with BC exhibited shape recovery over time. They were compressed to 12.5% and 50% compression and then fully unloaded. In the PA11 and PA11/3 wt.% BC meta-biocomposites, reinforced with GF, retain a measurable residual deformation. They were also compressed to 12.5% and 50% compression and then fully unloaded



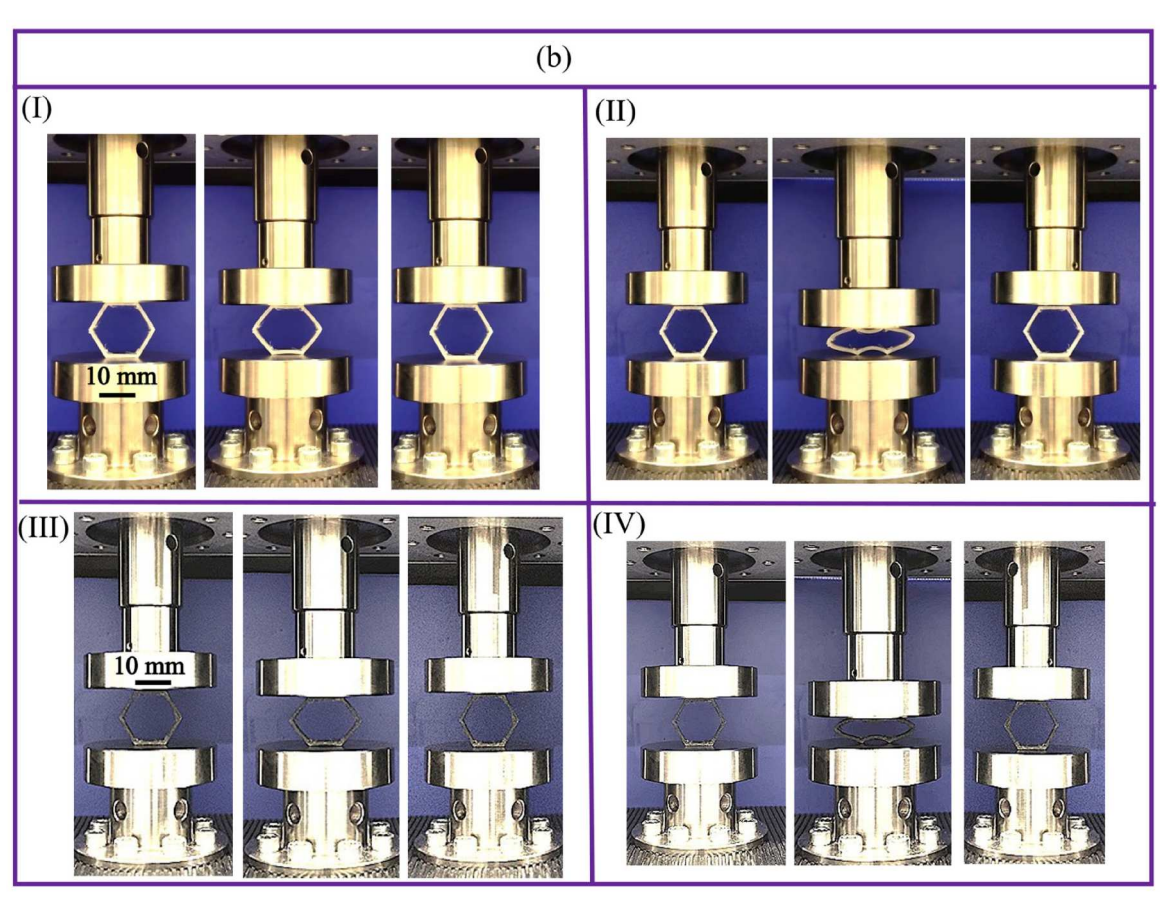


**Figure 19.** (a) 3D printed meta-bio-composites with a hexagonal cross-section; (b) configuration of PA11 under 12.5% and 50% compression (I & II), configuration of PA11 reinforced with BC under 12.5% and 50% compression (III & IV); (c) configuration of the PA11 reinforced with GF (V & VI) and PA11 reinforced with BC and GF (VII & VIII); (d, e) the force-displacement response of various meta-bio-composites under a loading-unloading-recovery cycle.

(Figure 19(c)). This permanent set is likely due to inelastic deformation of GF and micro- to macro-scale fibre damage.

Figures 19(d and e) highlights that incorporating BC and GF reinforcement significantly changes the mechanical response of these meta-structures. Reinforcement leads to higher stiffness (steeper loading curve slope), larger hysteresis loops, and greater peak forces. In

particular, BC and GF addition to PA11 and PA11/BC not only increases stiffness but also energy absorption/ dissipation capacity. PA11 and PA11/BC structures compressed to 50% show controlled force regulation with an almost linear response during loading, transitioning into a QZS stage where force remains nearly constant over a set deformation range (e.g. 8 mm for PA11 and PA11/3 wt.% BC). This QZS state lowers peak forces, improves

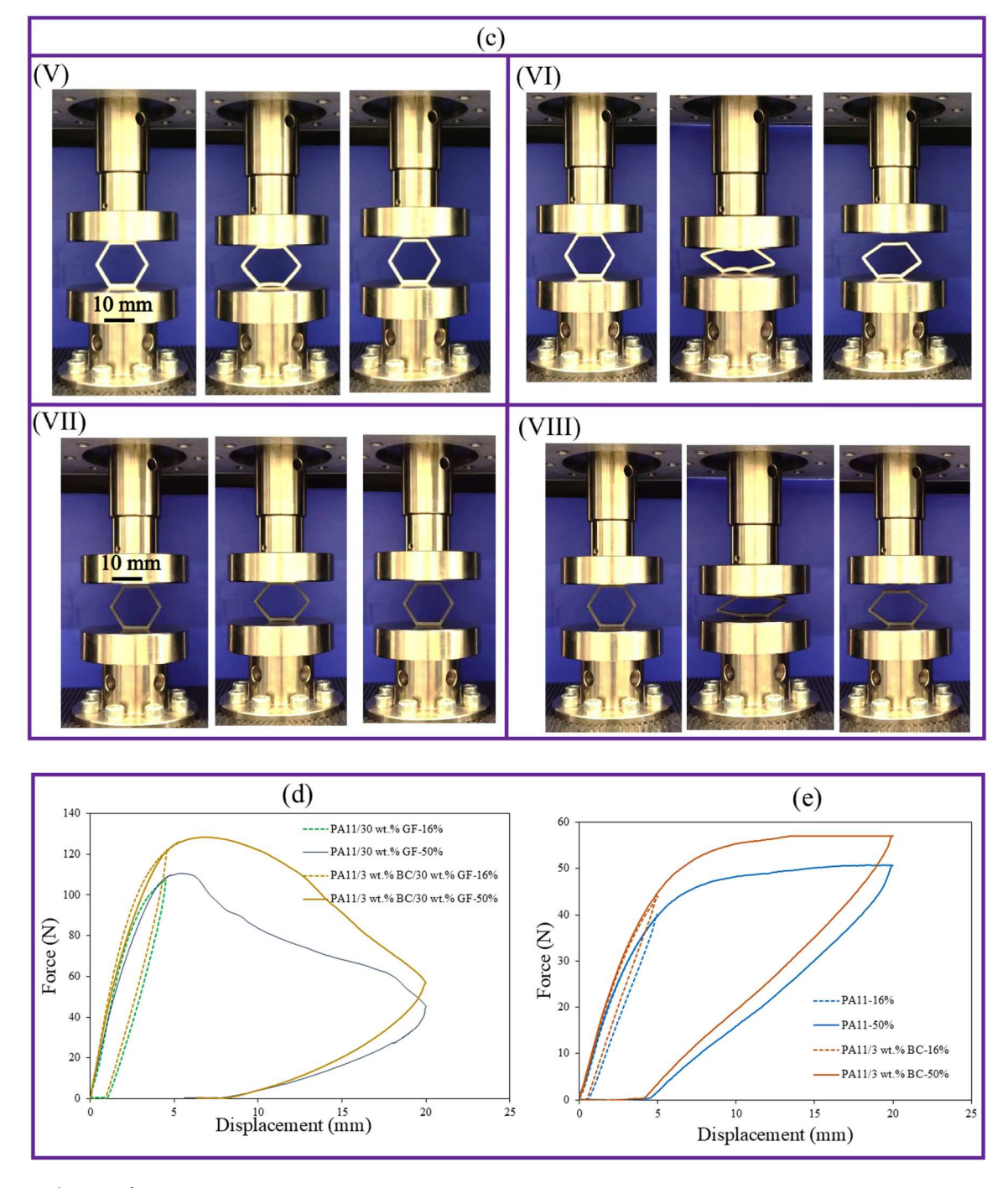


Figure 19 Continued

energy dissipation, limits load accumulation, and enhances stress relief. These benefits are valuable for impact mitigation, overload protection, and ergonomic comfort. However, PA11 and PA11/BC structures reinforced with high GF content tend to become more brittle. Restricted polymer chain mobility reduces controlled deformation, preventing a clear QZS stage.

Energy absorption and dissipation were evaluated through one complete loading-unloading cycleusing force-displacement hysteresis loops. In viscoelastic or hyper-elastic systems, the total absorbed energy is given by the area under the loading curve, dissipated energy by the enclosed loop area (irreversible deformation), and recoverable energy by the unloading curve area. In the research, the specific energy absorption (SEA) was calculated as the area under the loading curve up to the target strain, divided by the specimen mass, providing the energy absorbed per unit. More details on SEA calculation of the meta-bio-composites can be found in Bodaghi et al. [40]. SEA values were quantified

numerically from the experimental results (Figures 19(d and e)). The PA11 reinforced with GF and BC at 50% compression exhibited the highest SEA of 655 J/kg, with an increase of 145% compared to PA11 (267 J/kg), highlighting the strong synergistic effect of BC and GF. A similar was reported by Cheng et al. [46] showed that the energy absorption capacity of the 3D printed samples increased with the addition of natural reinforcement.

The strength-to-weight ratio, a key indicator for lightweight structural efficiency, exhibits an improvement with the addition of both BC and GF reinforcements. As shown in Table 4, the addition of BC enhanced the ratio, and the incorporation of GF leads to a significant increase in performance, particularly in the PA11/3 wt.% BC/30 wt.% GF sample at 50% compression, achieving the maximum strength-to-weight ratio of 700% compared to pure PA11. The BC fine dispersion within the PA11 matrix not only enhanced stress transfer efficiency and provided local stiffening, but also, BC contributes to structural integrity without adding excessive mass. Their porous structure promoted interfacial adhesion and energy dissipation under tensile loading. Notably, even at 3 wt.% BC, the ratio remains considerably higher than that of the PA11, confirming the effectiveness of bio-based reinforcements for applications where mechanical strength and lightweight design are simultaneously critical. However, PA11 and PA11/BC structures with high GF content significantly enhance mechanical properties but increase density and potential embrittlement. Restricted polymer chain mobility reduces controlled deformation, preventing a clear QZS stage. Therefore, an optimal GF persent must be selected to balance strength and toughness. This could be considered as future endeavour.

#### 5. Potential applications

The current findings support the development of a comprehensive database of PA11-based bio-composites aligned with sustainability goals. Bio-based PA11, compared with petroleum-derived plastics and many conventional polyamides, has a much lower environmental footprint and is not biodegradable like PLA, which is advantageous in durable products. In addition, the

**Table 4.** Strength-Weight ratio for the PA11 bio-composites.

Samples	Strength (KPa)	Mass (g)	Strength to weight ratio (KPa/N)
PA11	146	2.40	6.1
PA11/3 wt.% BC	181	2.48	7.29
PA11/30 wt.% GF	343	2.69	12.7
PA11/3 wt.% BC/30 wt.% BC	400	2.89	13.8

bio-composites help reduce reliance on virgin materials and support the recycling aspect of the circular economy. They combine high thermo-mechanical strength, effective impact-energy dissipation, mechanical compliance, and a OZS meta-structure that delivers a stable and comfortable load response. Moreover, the system improves flame retardancy and moisture management and, by using renewable resources such as bamboo charcoal, offers endof-life recovery options. These synergistic properties make the proposed meta-material suitable for a wide range of applications, such as transportation (automobile/motorcycle and their customisation), sports, and robotics. It is worth noting that the present metamaterial system was primarily designed and evaluated based on short-term mechanical properties and hydrophobic behaviour under various temperature conditions. For applications such as automobiles and robots that require long-term operation, the long-term durability, fatigue resistance, and stability of these bio-composite materials under harsh environments should be further examined. Future studies will focus on conducting cyclic fatigue (e.g. thermal cycling, humidity) and creep tests to comprehensively evaluate their durability and ensure stable long-term performance.

It should be finally mentioned that, in industries (such as automotive), PA11 is commonly used for mass production via injection moulding and other processes. However, for rapid prototyping of new products, lowcost on-site repair, and lightweight architectures like components for electric cars and robots, AM is a practical, low-cost alternative. FFF enables these use cases efficiently. Several simple, conceptual designs are discussed below, and a pictorial summary of application areas is provided in Figure 20.

#### 1) Rapid prototyping

Rapid prototyping accelerates product development by allowing quick validation of assembly and function, as well as accurate architectural/industrial design models. The main advantages are shorter development time and cost, fast iteration, and parallel testing before final production. In this context, FFF and in general AM enables the reproduction of spare parts for refurbishment projects, especially in the automobile and motorcycle sectors, where accurate remanufacture of scarce spares is needed. It also supports printer parts for tuning, aimed at decorative/aesthetic functions and customisation (Figure 20).

#### 1) Sports

Given the multifunctional performance of these biocomposites, they perform well under long contact with

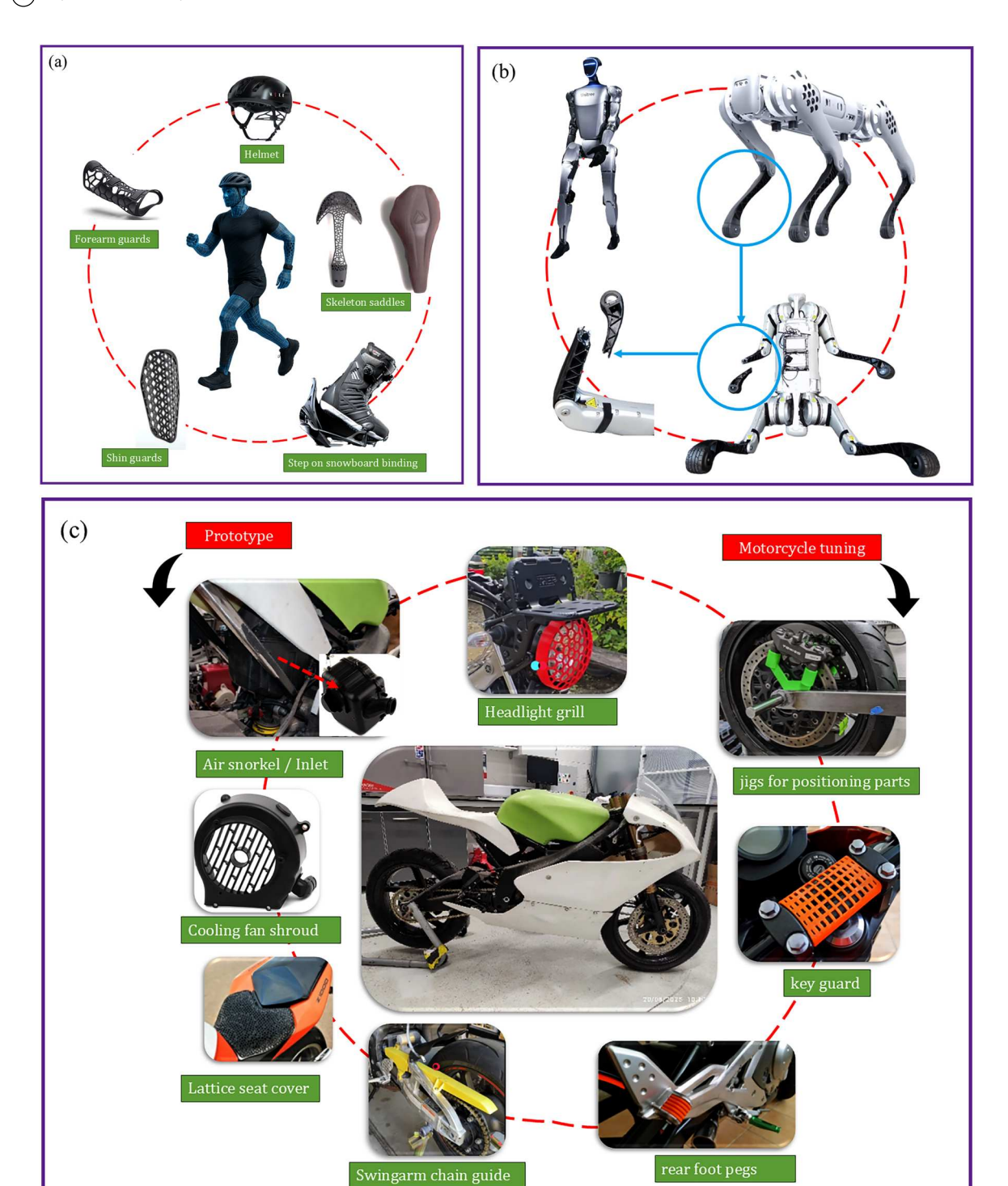


Figure 20. Illustration of potential application domains for the proposed bio-composite for a wide range of applications, including sport gears (a), robotic bodies (b), and transportation such as motorcycle parts (image: NTU-lab-made motorcycle) (c), and parts for prototyping and tuning cars (d).

skin and exposure to sweat or moisture in sport products (e.g. bicycle saddles, helmets, forearm guards, shin guards, and ski-boot frames (see Figure 20(a))). Hydrophobicity and moisture retention promote effective sweat wicking and improve skin comfort. The QZS meta-structure acts as an energy absorber and overload limiter, reducing impact forces while keeping a compact

form, well-suited to applications where safety and comfort must coexist.

#### 2) Robotics

With the rapid growth of robots from humanoids and quadrupeds, the proposed bio-composites enable



Figure 20 Continued

lightweight parts with high specific strength for robotics. In addition, in the FFF method, compared to other methods, a new part can be designed and reprinted quickly and at low cost if a part fails during service to repair the system and restore operation. As illustrated in Figure 20(b), damaged components in a quadruped dog robot (e.g. our recently broken leg) can be replaced by FFF parts without relying on casting or injection moulding. This approach supports the circular economy by enabling on-site repairs, shortening downtime, design freedom, and reducing dependency on supply chains.

#### 3) Transportation

Applications of FFF processes for transportation parts were previously limited by material requirements, mechanical, thermal, and chemical responses. To overcome these limits, fibre reinforcements have been added to improve mechanical properties. In transportation, including automobiles and motorcycles, for both power-train-adjacent and protective components, PA11 reinforced with glass fibre and bamboo is a reliable option. It offers multifunctional performance: high strength and resistance to moisture, heat, impact, and flame retardancy adds a layer of thermal safety. Together

with the tuneable mechanical response of the metastructure, these features yield a material that is resilient and efficient, and suitable for real-world scenarios with thermal risk. In addition, the QZS meta-structure acts as an energy absorber and overload limiter, reducing impact forces (Figures 20(c and d)).

Beyond the unique structural features, the PA11 reinforced with bamboo and glass fibre also provides important performance benefits. Hydrophobicity and moisture repellence promote effective sweat wicking and lower the risk of chafing; therefore, it is suitable for long-term use in warm or humid environments. Flame-retardant behaviour adds a critical layer of thermal safety, especially for helmets and transportation parts where heat or ignition may occur. Together with the meta-structure's mechanical compliance, these properties yield a meta-material that is mechanically robust, thermally resilient, and resistant to ignition, making it suitable for a wide range of real-world applications.

#### 6. Conclusion

The demand for high-performance, sustainable materials has driven the development of bio-composites that balance mechanical strength, flame retardancy, and



energy absorption/dissipation. This study introduces a PA11-based bio-composite reinforced with bamboo charcoal and glass fibre, demonstrating exceptional thermo-mechanical performance, hydrophobicity, processability, and environmental benefits. The key findings and contributions are summarised as follows:

- The incorporation of 3 wt.% BC moderate reduces FFF warpage in PA11, lowering the average from 3.81 mm to 2.58 mm, while the 3 wt.% BC/30 wt.% GF samples nearly eliminate visible deformation (0.1 mm).
- SEM micrographs confirm uniform BC particle dispersion and strong PA11 fibre interfaces; the hybrid architecture improves crack deflection, fibre pull-out, and energy-dissipating mechanisms.
- Water contact angles increase from 62.25 ° (PA11) to 78.17 ° (bio-composite), demonstrating enhanced hydrophobicity and improved moisture resistance for automotive applications.
- 4. DMA shows that the bio-composite (3 wt.% BC/30 wt.% GF) retains about 1 GPa storage modulus at 100°C (versus 0.10 GPa for PA11), indicating superior thermal-softening resistance.
- UL-94 horizontal burning rates decrease by up to 61.9% in reinforced samples and in UL-94 vertical, attaining a V-2 rating and an LOI of 29.1 vol.%, evidencing marked flame-retardant improvements with BC and GF additives.
- 6. At 23°C, the bio-composite (3 wt.% BC/30 wt.% GF) delivers a 194% increase in ultimate tensile strength (26–76.5 MPa) and a 361% enhancement in Young's modulus (1.7–7.85 GPa) compared to PA11.
- Flexural performance shows up to a 292% increase in ultimate flexural stress and a 200% increase in modulus for the bio-composite (3 wt.% BC/30 wt.% GF), confirming synergistic reinforcement in bending.
- 8. Impact energy absorption rises by 443% (0.32–1.74 kJ/m²) and Shore-A hardness modestly increases (94–100 ShA) in the hybrid bio-composite without embrittlement.
- 9. BC provides stiffness enhancements, GF supplies high strength and dimensional stability, and their combination yields balanced mechanical, thermal, and flame-resistant properties. While GF serves as a mechanical benchmark to validate the reinforcement potential of bio-derived BC, the hybrid formulation demonstrates that the inclusion of BC meaningfully contributes to printability, dimensional stability, and environmental sustainability without relying solely on nonrenewable fibres.

10. The bio-based PA11/BC/GF composites indicate a sustainable, high-performance solution for lightweight sport, robotic, and transportation components. Therefore, the hybrid design can be viewed as a transitional, benchmark-driven step toward next-generation green composites capable of replacing purely glass-fibre-reinforced systems.

Finally, it should be mentioned that while the biocomposites have been developed for FFF 3D printing, their pellet form could be used as raw materials for inject moulding as well for a mass production purpose.

#### **Author contributions**

CRediT: Kaveh Rahmani: Conceptualisation, Data curation, Formal analysis, Investigation, Methodology, Validation, Visualisation, Writing – original draft, Writing – review & editing; Callum Branfoot: Investigation, Methodology, Supervision, Writing – review &editing; Mahdi Bodaghi: Conceptualisation, Funding acquisition, Investigation, Methodology, Project administration, Resources, Supervision, Writing – original draft, Writing – review & editing.

#### **Acknowledgements**

The authors acknowledge the support by the Engineering and Physical Sciences Research Council (EPSRC), the EPSRC's Innovation Launchpad Network+ Researcher in Residence scheme, Nottingham Trent University, and National Composites Centre.

#### **Disclosure statement**

No potential conflict of interest was reported by the author(s).

#### **Funding**

This work was supported by the Engineering and Physical Sciences Research Council (EPSRC) [award number: EP/Y011457/1, project: I5M]; and the EPSRC's Innovation Launchpad Network+Researcher in Residence scheme [grant numbers: EP/W037009/1, EP/X528493/1; award number: RIR26C230615-6, project: BIO-CYCLE, researcher: Mahdi Bodaghi].

#### **Data availability statement**

The raw test data supporting the findings of this study are openly available in Zenodo at: https://doi.org/10.5281/zenodo.17228623

#### **ORCID**

Mahdi Bodaghi Dhttp://orcid.org/0000-0002-0707-944X



#### References

- [1] Russo P, Simeoli G, Vitiello L, et al. Bio-polyamide 11 hybrid composites reinforced with basalt/flax interwoven fibers: A tough green composite for semi-structural applications. Fibers. 2019;7(5):41. doi:10.3390/fib7050041
- [2] Bocz KB. Development of environmentally friendly flame retarded polymer composites. Hungary: Budapest University of Technology and Economics; 2015.
- [3] Feldmann M, Bledzki AK. Bio-based polyamides reinforced with cellulosic fibres-processing and properties. Compos Sci Technol. 2014:100:113-120. doi:10. 1016/i.compscitech.2014.06.008
- [4] Krishna S, Sreedhar I, Patel CM. Molecular dynamics simulation of polyamide-based materials-a review. Comput Mater Sci. 2021;200:110853. doi:10.1016/j.commatsci. 2021.110853
- [5] Taneepanichskul N, Purkiss D, Miodownik M. A review of sorting and separating technologies suitable for compostable and biodegradable plastic packaging. Front Sust. 2022;3:901885. doi:10.3389/frsus.2022.901885
- [6] Doğru A, Seydibeyoğlu MÖ, Ayranci C. The effect of interface enhancement on the mechanical properties of fibrereinforced PA6 matrix composites in material extrusionbased additive manufacturing. Prog Addit Manuf. 2025;10(1):361-374. doi:10.1007/s40964-024-00628-7
- [7] Ranakoti L, Gangil B, Mishra SK, et al. Critical review on polylactic acid: properties, structure, processing, biocomposites, and nanocomposites. Materials. 2022;15(12): 4312. doi:10.3390/ma15124312
- [8] Autay R, Missaoui S, Mars J, et al. Mechanical and tribological study of short glass fiber-reinforced PA 66. Polym 2019;27(9):587-596. doi:10.1177/ Polym Compos. 0967391119853956
- [9] Dechet MA, Lanzl L, Werner Y, et al. (2019). Manufacturing and application OF PA11-glass fiber composite particles for selective laser sintering. In: Solid Freeform Fabrication 2019: Proceedings of the 30th Annual International.
- [10] Bagrov D, Perunova S, Pavlova E, et al. Wetting of electrospun nylon-11 fibers and mats. RSC Adv. 2021;11(19): 11373-11379. doi:10.1039/D0RA10788C
- [11] da Costa Mattos H, Brandão J, Amorim F, et al. A unified expression to estimate the stress-strain curve of polyamides at different temperatures. Mater Res Exp. 2018;6(1):015304. doi:10.1088/2053-1591/aae564
- [12] Sabet M. Advancements in halogen-free polymers: exploring flame retardancy, mechanical properties, sustainability, and applications. Polym-Plast Technol Mater. 2024;63(13):1794-1818. doi:10.1080/25740881.2024. 2359633
- [13] Liu BW, Zhao HB, Wang YZ. Advanced flame-retardant methods for polymeric materials. Adv 2022;34(46):2107905. doi:10.1002/adma.202107905
- [14] Ahmad MN, Ishak MR, Mohammad Taha M, et al. A review of natural fiber-based filaments for 3D printing: filament fabrication and characterization. Materials. 2023:16(11): 4052. doi:10.3390/ma16114052
- [15] Wu Q, Liu Y, Han Z, et al. Surface modification of bamboo fibers by diammonium phosphate and their applications in flame retardant thermoplastic polyurethane. J Appl Polym Sci. 2021;138(25):50606. doi:10.1002/app.50606

- [16] Chen Q, Zhang R, Wang Y, et al. The effect of bamboo charcoal on water absorption, contact angle, and the physicalmechanical properties of bamboo/low-density polyethylene composites. BioResources. 2016;11(4):9986-10001.
- [17] Sergi C, Vitiello L, Dang P, et al. Low molecular weight biopolyamide 11 composites reinforced with flax and intraply flax/basalt hybrid fabrics for eco-friendlier transportation components. Polymers. 2022;14(22):5053. doi:10. 3390/polym14225053
- [18] Oliver-Ortega H, Méndez JA, Mutjé P, et al. Evaluation of thermal and thermomechanical behaviour of bio-based polyamide 11 based composites reinforced with lignocellulosic fibres. Polymers. 2017;9(10):522. doi:10.3390/ polym9100522
- [19] Wambua P, Ivens J, Verpoest I. Natural fibres: can they replace glass in fibre reinforced plastics? Compos Sci Technol. 2003;63(9):1259-1264. doi:10.1016/S0266-3538 (03)00096-4
- [20] Maiti S, Islam MR, Uddin MA, et al. Sustainable fiberreinforced composites: a review. Adv Sust Syst. 2022;6(11):2200258. doi:10.1002/adsu.202200258
- [21] Sałasińska K, Ortega Z, Jurczyk-Kowalska M, et al. Biosourced flame retardant systems for polymers: the influence of chemical modification of giant reed on thermal stability and flammability of PA11. J Therm Anal Calorim. 2025: 1-14.
- [22] Qi S, Gao X, Su Y, et al. Effect of carbon nanotubes on mechanical properties of polyamide 12 parts by fused filament fabrication. Polymer. 2022;247:124784. doi:10. 1016/j.polymer.2022.124784
- [23] Jindal S, Manzoor F, Haslam N, et al. 3D printed composite materials for craniofacial implants: current concepts, challenges and future directions. Int J Adv Manuf Technol. 2021;112(3):635-653. doi:10.1007/s00170-020-06397-1
- [24] Tey WS, Cai C, Zhou K. A comprehensive investigation on 3D printing of polyamide 11 and thermoplastic polyurethane via multi jet fusion. Polymers. 2021: 13(13):2139. doi:10.3390/polym13132139
- [25] Martino L, Basilissi L, Farina H, et al. Bio-based polyamide 11: synthesis, rheology and solid-state properties of star structures. Eur Polym J. 2014;59:69-77. doi:10.1016/j. eurpolymj.2014.07.012
- [26] Rahmani K, Branfoot C, Karmel S, et al. Flexible bio-composites with continuous natural fibre and bamboo charcoal: enhanced flame retardancy, mechanical resilience, energy-absorbing & printability performance. Virtual doi:10.1080/ Phys Prototyp. 2025;20(1):e2534845. 17452759.2025.2534845
- [27] Wang Y, Li Z, Li X, et al. Effect of the temperature and strain rate on the tension response of uncured rubber: experiments and modeling. Mech Mater. 2020; 148:103480. doi:10.1016/j.mechmat.2020.103480
- [28] Alarifi IM. Revolutionising fabrication advances and applications of 3D printing with composite materials: a review. Virtual Phys Prototyp. 2024;19(1):e2390504. doi:10.1080/ 17452759.2024.2390504
- [29] Schmutzler C, Stiehl TH, Zaeh MF. Empirical process model for shrinkage-induced warpage in 3D printing. Rapid Prototyp J. 2019;25(4):721-727. doi:10.1108/RPJ-04-2018-0098
- [30] Schmutzler C, Zimmermann A, Zaeh MF. Compensating warpage of 3D printed parts using free-form deformation.



- Procedia Cirp. 2016;41:1017–1022. doi:10.1016/j.procir. 2015.12.078
- [31] Gaspar-Cunha A, Melo J, Marques T, et al. A review on injection molding: conformal cooling channels, modelling, surrogate models and multi-objective optimization. Polymers. 2025;17(7):919. doi:10.3390/polym17070919
- [32] Annicchiarico D, Alcock JR. Review of factors that affect shrinkage of molded part in injection molding. Mater Manuf Processes. 2014;29(6):662–682. doi:10.1080/ 10426914.2014.880467
- [33] Chenrayan V, Kanaginahal G, Shahapurkar K, et al. Analytical modeling and experimental estimation of the dynamic mechanical characteristics of green composite: caesalpinia decapetala seed reinforcement. Polym Eng Sci. 2024;64(3):1096–1109. doi:10.1002/pen.26599
- [34] Barczewski M, Hejna A, Andrzejewski J, et al. The recyclability of fire-retarded biobased polyamide 11 (PA11) composites reinforced with basalt fibers (BFs): the influence of reprocessing on structure, properties, and fire behavior. Molecules. 2024;29(13):3233. doi:10.3390/molecules29133233
- [35] Ravanbod S, Rahmani K, Karmel S, et al. From coral to control: bio-inspired, 3D-printable metamaterials with tuneable quasi-zero stiffness and multi-functional bio-composites. Mater Des. 2025: 114398. doi:10.1016/j.matdes.2025. 114398
- [36] Cheng P, Wang K, Chen X, et al. Interfacial and mechanical properties of continuous ramie fiber reinforced biocomposites fabricated by in-situ impregnated 3D printing. Ind Crops Prod. 2021;170:113760. doi:10.1016/j.indcrop. 2021.113760
- [37] Rahmani K, Malekmohammadi H, Haque A, et al. Bio-composite design and 3D printing of soft multi-functional meta-structures with tuneable quasi-constant force. Appl Mater Today. 2025;47:102961. doi:10.1016/j.apmt. 2025.102961
- [38] Bodaghi M, Rahmani K, Dezaki ML, et al. 3D/4D printed bio-composites reinforced by bamboo charcoal and

- continuous flax fibres for superior mechanical strength, flame retardancy and recoverability. Polym Test. 2025;143:108709. doi:10.1016/j.polymertesting.2025. 108709
- [39] Shaw MT, MacKnight WJ. *Introduction to polymer viscoelasticity*. John Wiley & Sons; 2018.
- [40] Moradi M, Karami Moghadam M, Shamsborhan M, et al. The synergic effects of FDM 3D printing parameters on mechanical behaviors of bronze poly lactic acid composites. J Compos Sci. 2020;4(1):17. doi:10.3390/ ics4010017
- [41] Caminero M, Chacón J, García-Moreno I, et al. Impact damage resistance of 3D printed continuous fibre reinforced thermoplastic composites using fused deposition modelling. Compos B Eng. 2018;148:93–103. doi:10.1016/i.compositesb.2018.04.054
- [42] Vitiello L, Russo P, Papa I, et al. Flexural properties and low-velocity impact behavior of polyamide 11/basalt fiber fabric laminates. Polymers. 2021;13(7):1055. doi:10. 3390/polym13071055
- [43] Günaydın K, Rea C, Kazancı Z. Energy absorption enhancement of additively manufactured hexagonal and re-entrant (auxetic) lattice structures by using multi-material reinforcements. Addit Manuf. 2022;59: 103076. doi:10.1016/j.addma.2022.103076
- [44] Khatri NR, Egan PF. Energy absorption of 3D printed ABS and TPU multimaterial honeycomb structures. 3D Print Addit Manuf. 2024;11(2):e840–e850. doi:10.1089/3dp. 2022.0196
- [45] Lalegani Dezaki M, Branfoot C, Baxendale J, et al. Biobased gradient composites for 3D/4D printing with enhanced mechanical, shape memory, and flame-retardant properties. Macromol Mater Eng. 2025;310(6): 2400276. doi:10.1002/mame.202400276
- [46] Cheng P, Peng Y, Wang K, et al. Quasi-static penetration property of 3D printed woven-like ramie fiber reinforced biocomposites. Compos Struct. 2023;303:116313. doi:10. 1016/j.compstruct.2022.116313